

Local fermion density in inhomogeneous free-fermion chains: a discrete WKB approach

Martín Zapata^{1*}, Federico Finkel^{2†} and Artemio González-López^{2‡}

1 Theory Division, Max Planck Institute of Quantum Optics, D-85748 Garching, Germany

2 Departamento de Física Teórica, Facultad de Ciencias Físicas, Universidad Complutense de Madrid, Plaza de las Ciencias 1, 28040 Madrid, Spain

* martin.zapata@mpq.mpg.de, † ffinkel@ucm.es, ‡ artemio@ucm.es

Abstract

We introduce a novel analytical approach for studying free-fermion (XX) chains with smoothly varying, site-dependent hoppings and magnetic fields. Building on a discrete WKB-like approximation applied directly to the recurrence relation for the single-particle eigenfunctions, we derive a closed-form expression for the local fermion density profile as a function of the Fermi energy, which is valid for arbitrary fillings, hopping amplitudes and magnetic fields. This formula reproduces the depletion and saturation effects observed in previous studies of inhomogeneous free-fermion chains, and provides a theoretical framework to understand entanglement entropy suppression in these models. We demonstrate the accuracy of our asymptotic formula in several chains with different hopping and magnetic field profiles. Our findings are thus the first step towards an analytical treatment of entanglement in free-fermion chains beyond the reach of conventional field-theoretic techniques.

Contents

1	Introduction	2
2	Preliminaries	4
3	Single-particle WKB wave functions	6
4	Fermionic density profile	11
5	Examples	18
5.1	The homogeneous chain	18
5.2	The Krawtchouk chain	20
5.3	The rainbow chain	24
5.4	The cosine chain	28
5.5	An asymmetric cosine chain	30
6	Conclusions and outlook	32
References		33

1 Introduction

The study of one-dimensional quantum systems is central to our understanding of many-body physics, particularly in the context of condensed matter physics and quantum entanglement. In recent years, attention has increasingly focused on inhomogeneous spin chains, in which hopping amplitudes and external magnetic fields vary across the lattice, due to their relevance in cold atomic systems on optical lattices [1, 2], engineered quantum simulators [3–5], and the study of entanglement in non-uniform environments [6–8]. Among these chains, the inhomogeneous version of the spin- $\frac{1}{2}$ Heisenberg XX chain [9] occupies a prominent place, both for its conceptual simplicity and its connections to free fermion systems. With open boundary conditions, and in the presence of an external magnetic field, the Hamiltonian of this model can be taken as¹

$$H = \frac{1}{2} \sum_{n=0}^{N-2} J_n (\sigma_n^x \sigma_{n+1}^x + \sigma_n^y \sigma_{n+1}^y) + \frac{1}{2} \sum_{n=0}^{N-1} B_n (1 - \sigma_n^z), \quad (1)$$

where σ_n^α ($\alpha = x, y, z$) denotes the Pauli matrix σ^α acting on the n -th site. As is well known, this Hamiltonian can be mapped to the fermionic Hamiltonian

$$H = \sum_{n=0}^{N-2} J_n (c_n^\dagger c_{n+1} + \text{H.c.}) + \sum_{n=0}^{N-1} B_n c_n^\dagger c_n \quad (2)$$

through the Jordan–Wigner transformation [11]

$$c_n \mapsto \prod_{j=0}^{n-1} \sigma_j^z \cdot \sigma_n^+, \quad \sigma_n^\pm := \frac{1}{2} (\sigma_n^x \pm i\sigma_n^y). \quad (3)$$

Since c_n^\dagger creates a (spinless) fermion at site n , the Hamiltonian (2) describes a system of hopping fermions with hopping amplitude J_n and chemical potential B_n . As explained in the next section, the full spectrum of the Hamiltonian (2) consists of excitations of single-particle energy modes. Moreover, since the Hamiltonian (2) conserves particle number, it is possible to construct a basis of energy eigenstates with well-defined total fermion number M and filling fraction $\nu = M/N \in [0, 1]$.

The XX model is one of the few systems for which the (bipartite) entanglement entropy of energy eigenstates can be numerically evaluated for a large number of spins [12–14]. In general, given a bipartition of a quantum system into two disjoint blocks A and B , the bipartite entanglement entropy S of pure state $|\psi\rangle$ of the whole system is defined by

$$S = s[\rho_A], \quad \rho_A = \text{tr}_B(\rho), \quad (4)$$

where $\rho = |\psi\rangle\langle\psi|$ is the density matrix of the state $|\psi\rangle$, ρ_A is the (in general, mixed) reduced density matrix of subsystem A , and s is an entropy functional (usually the Rényi entropy [15]). A particularly intriguing phenomenon observed in inhomogeneous XX chains is the suppression of bipartite entanglement entropy at certain block sizes for fillings $\nu \neq 1/2$ and/or inhomogeneous magnetic fields [16], in contrast to the behavior observed in the homogeneous case ($J_n = J, B_n = B$). Mula et al. [17] provided a natural explanation of this phenomenon in terms of an exponential reduction, termed ‘depletion’, of the local fermionic density. Using field-theoretic techniques, these authors derived an approximate heuristic formula for the occupation profile, valid only in the low-filling limit and for zero magnetic field. This formula

¹As shown in Ref. [10], all the models obtained replacing J_n by $\varepsilon_n J_n$, where $\varepsilon_n \in \{\pm 1\}$ is a site dependent sign, are actually unitarily equivalent.

was able to account for depletion in this regime, and in particular to predict the location of the depletion intervals in several simple examples. Nevertheless, a general, analytically tractable approach valid for arbitrary fillings/magnetic fields has so far remained elusive.

In this paper we introduce a novel method for studying the local density of inhomogeneous free-fermion chains in the thermodynamic limit. Our main idea is to directly analyze the behavior of the model's single-particle eigenfunctions in the large N limit, avoiding intermediate approximations. In particular, we do not base our analysis (as is usually done in the literature; see, e.g., refs. [7, 8, 17, 18]) on field-theoretic techniques, which often rely on approximations valid only in the absence of a magnetic field, and either near the critical regime (half filling) or at low filling. Our approach is rather based on applying a WKB-like approximation to the three-term recurrence relation satisfied by the single-particle eigenfunctions of the discrete model in the large N limit. In this way we obtain continuous ('WKB') approximations to these eigenfunctions, which we then use to derive an asymptotic expression for the fermionic density as a function of the Fermi energy ε_F valid for arbitrary filling fractions and/or external magnetic fields. More precisely, we show that the average occupation number at an arbitrary Fermi energy ε_F , hopping J_n and magnetic field B_n is approximately given by

$$\langle c_n^\dagger c_n \rangle \simeq \begin{cases} 0, & \varepsilon_F \leq B_n - 2J_n, \\ \frac{1}{\pi} \arccos\left(\frac{B_n - \varepsilon_F}{2J_n}\right), & B_n - 2J_n \leq \varepsilon_F \leq B_n + 2J_n, \\ 1, & \varepsilon_F \geq B_n + 2J_n. \end{cases} \quad (5)$$

In the absence of an external magnetic field our result agrees with ref. [17] in the low filling limit, while at high filling we find a mirror image of depletion, which we may call 'saturation', that the heuristic formula in the last reference cannot reproduce. In particular, eq. (5) is able to accurately determine the saturation regions, which can appear even for relatively low values of the filling fraction in sufficiently strong magnetic fields. We validate our analytical predictions through extensive numerical simulations across several classes of inhomogeneous chains, including the rainbow, Krawtchouk, cosine, and Rindler² chains. In all cases, eq. (5) is in excellent agreement with the numerical results over the whole range of energies/filling fractions, hoppings and magnetic fields involved. Beyond its immediate applicability to fermion density profiles, our method is also a promising starting point for deriving asymptotic formulas for correlation matrices and entanglement entropies in inhomogeneous fermionic chains, particularly where conformal field theory methods are not directly applicable due to the lack of scale invariance.

Our paper is structured as follows. In section 2 we collect several well-known preliminary results used throughout the paper. In particular, we recall the role of single-particle states in the exact diagonalization of the model, and its connections with the theory of orthogonal polynomials. In section 3 we apply the discrete WKB approximation to the recurrence relation satisfied by the single-particle eigenfunctions. We derive approximate WKB wave functions, which are then used in section 4 to obtain accurate asymptotic formulas for the fermionic density profile and the filling fraction in the thermodynamic limit. In section 5 we apply our method to several well-known types of inhomogeneous XX chains like the Krawtchouk, rainbow, and cosine chains, including an asymmetric generalization of the latter. Finally, in section 6 we summarize the paper's main results and discuss natural directions for future work suggested by our findings.

²For the Rindler chain, see the Supplementary Material.

2 Preliminaries

Let us first briefly recall how to diagonalize the fermionic Hamiltonian (2). To this end, note that this Hamiltonian is a quadratic function of fermionic operators:

$$H = \sum_{n,m=0}^{N-1} H_{nm} c_n^\dagger c_m, \quad H_{nm} := J_n \delta_{m,n+1} + J_{n-1} \delta_{m,n-1} + B_n \delta_{nm}, \quad (6)$$

where $J_{-1} = J_{N-1} = 0$. Using vector notation

$$\mathbf{c} = (c_1, \dots, c_N)^\top, \quad \mathbf{c}^\dagger = (c_1^\dagger, \dots, c_N^\dagger), \quad \mathbf{H} = (H_{nm}),$$

we can more concisely write

$$H = \mathbf{c}^\dagger \mathbf{H} \mathbf{c}.$$

Let $|n\rangle = c_n^\dagger |\text{vac}\rangle$ denote the state with exactly one fermion at site n , so that

$$\{|n\rangle : n = 0, \dots, N-1\}$$

is an orthonormal basis of the single-particle subspace. We then have

$$H_{nm} = \langle n | H | m \rangle,$$

and thus \mathbf{H} is the matrix of the restriction of H to the single-particle sector.

Since the matrix \mathbf{H} is real and symmetric, it can be diagonalized by means of a suitable real orthogonal matrix $\Phi = (\Phi_{nk})$. More precisely, setting

$$\tilde{\mathbf{c}} = \Phi^\top \mathbf{c}$$

we have

$$H = \tilde{\mathbf{c}}^\dagger \tilde{\mathbf{H}} \tilde{\mathbf{c}}, \quad \text{with} \quad \tilde{\mathbf{H}} = \Phi^\top \mathbf{H} \Phi = \text{diag}(\varepsilon_0, \dots, \varepsilon_{N-1}), \quad (7)$$

where $\varepsilon_0 < \dots < \varepsilon_{N-1}$ are the eigenvalues of \mathbf{H} —i.e., the single-particle energies. The new operators are still fermionic by virtue of the orthogonality of Φ . The operator \tilde{c}_k^\dagger creates a single fermion with well-defined energy ε_k , i.e., a single-particle energy mode. Since, by eq. (7),

$$H = \sum_{k=0}^{N-1} \varepsilon_k \tilde{c}_k^\dagger \tilde{c}_k, \quad (8)$$

the eigenstates of H can therefore be constructed by applying the operators \tilde{c}_k^\dagger to the vacuum state $|\text{vac}\rangle$, annihilated by all \tilde{c}_k . In other words, the states

$$|n_0, n_1, \dots, n_k\rangle := \tilde{c}_{n_0}^\dagger \tilde{c}_{n_1}^\dagger \cdots \tilde{c}_{n_k}^\dagger |\text{vac}\rangle, \quad 0 \leq n_0 < \dots < n_k \leq N-1, \quad (9)$$

are eigenstates of H with energies

$$E(n_0, n_1, \dots, n_k) = \sum_{j=0}^k \varepsilon_{n_j}, \quad (10)$$

and they form an orthonormal basis of the Hilbert space of H . Thus the full spectrum of H is obtained by exciting a number of single-particle energy modes.

It is well known that the eigenvectors $\phi_n(\varepsilon_k) := \Phi_{nk}$ are related to the family of monic orthogonal polynomials $\{P_n(\varepsilon)\}_{n=0}^N$ defined recursively via

$$P_{n+1}(\varepsilon) = (\varepsilon - b_n) P_n(\varepsilon) - a_{n-1} P_{n-1}(\varepsilon), \quad \text{with} \quad P_{-1}(\varepsilon) = 0, \quad P_0(\varepsilon) = 1,$$

where

$$a_n = J_n^2, \quad b_n = B_n$$

(see, e.g. [10, 16, 19]). Specifically, $\phi_n(\varepsilon_k) \propto P_n(\varepsilon_k)$, and the spectrum of the single-particle Hamiltonian coincides with the set of roots of the *critical polynomial* P_N . This equivalence has, for instance, aided in the classification of inhomogeneous XX chains of different types [10] and provided some exact spectra [16, 19–21]. It also guarantees that the single-particle eigenstates are non-degenerate.

If $M = 0, \dots, N$, we define the M -filled state $|M\rangle$ as the state obtained by exciting the lowest M single-particle energy modes:

$$|M\rangle = \prod_{k=0}^{M-1} \tilde{c}_k^\dagger |\text{vac}\rangle. \quad (11)$$

In particular, the system's ground state is the state $|M\rangle$ for which $\varepsilon_i < 0$ for $i = 0, \dots, M-1$ and $\varepsilon_M > 0$ (of course, the ground state is twice degenerate if there happens to be a zero mode). The correlation matrix $\mathbf{C} = (C_{nm})$ for this state $|M\rangle$ is defined by

$$C_{nm} := \langle M | c_n^\dagger c_m | M \rangle = \sum_{k=0}^{M-1} \Phi_{nk} \Phi_{mk}, \quad (12)$$

where the last equality follows from the identity

$$\langle M | \tilde{c}_k^\dagger \tilde{c}_q | M \rangle = \delta_{kq} \chi_M(k),$$

with

$$\chi_M(k) = \begin{cases} 1, & k \in \{0, \dots, M-1\}, \\ 0, & k \notin \{0, \dots, M-1\}. \end{cases}$$

As is well known [12–14], when the chain is in one of the states $|M\rangle$ defined above the entanglement entropy S_A of a block A of L spins can be expressed in terms of the eigenvalues λ_l (with $l = 0, \dots, L-1$) of the $L \times L$ truncated correlation matrix $\mathbf{C}_A = (C_{nm})_{n,m \in A}$ through the formula³

$$S_A = \sum_{l=0}^{L-1} s^{(2)}(\lambda_l), \quad (13)$$

where $s^{(2)}$ is the binary entropy associated to the entropy functional S .

As mentioned in the introduction, in this work we shall be mainly concerned with the diagonal elements of the (full) correlation matrix

$$C_{nn} = \langle M | c_n^\dagger c_n | M \rangle = \sum_{k=0}^{M-1} \Phi_{nk}^2 =: \langle c_n^\dagger c_n \rangle, \quad n = 0, \dots, N-1, \quad (14)$$

which provide the expectation value of the n -th site occupation number when the system is in the M -filled state $|M\rangle$. Although in this paper we shall not deal with the entanglement entropy, it is perhaps of interest to briefly explain how the entanglement entropy depletion arises from the depletion/saturation of occupation. To this end, note that since

$$0 = \langle c_n^\dagger c_n \rangle = \|c_n | M \rangle\|^2 \implies c_n | M \rangle = 0,$$

³More precisely, the following formula is valid if the entropy functional S is additive, as is the case for the Rényi and von Neumann entropies.

if (for instance) $\langle c_n^\dagger c_n \rangle$ vanishes for $n = 0, \dots, L-1$ the state $|M\rangle$ is the tensor product of the vacuum $\otimes_{n=0}^{L-1} |\text{vac}\rangle_n$ at sites $0, \dots, L-1$ with a pure state in the Hilbert space of the remaining sites. As a consequence, the entanglement entropy of a block $\{0, \dots, r-1\}$ with $r \leq L$ spins vanishes. The same conclusion holds if $\langle c_n^\dagger c_n \rangle = 1$ for $n = 0, \dots, L-1$, since

$$1 = \langle c_n^\dagger c_n \rangle = 1 - \langle c_n c_n^\dagger \rangle \implies 0 = \langle c_n c_n^\dagger \rangle = \|c_n^\dagger |M\rangle\|^2 \implies c_n^\dagger |M\rangle = 0,$$

and hence in this case $|M\rangle$ is the tensor product of the fully occupied state $\otimes_{n=0}^{L-1} |f\rangle_n$ with a pure state in the Hilbert space of the sites $L, \dots, N-1$.

3 Single-particle WKB wave functions

While the properties discussed in the previous section are valid in general, when trying to derive analytical results we will concern ourselves with a limited class of chains, with slowly varying hoppings and external magnetic field strength. More concretely, we introduce an arbitrarily small lattice spacing a and define the variable $x = na \in [0, \ell]$, such that the chain's length $\ell = Na$ remains finite as $a \rightarrow 0$ and $N \rightarrow \infty$. In this way, in the thermodynamic limit we can regard x as a continuous coordinate along the chain. We will assume that J_n and B_n converge pointwise to sufficiently smooth functions

$$J_n \xrightarrow[a \rightarrow 0]{} J(x), \quad B_n \xrightarrow[a \rightarrow 0]{} B(x), \quad (15)$$

where our notion of pointwise convergence for lattice functions $f_{n;N}$ will be

$$\lim_{\substack{N \rightarrow \infty \\ na \rightarrow x}} f_{n;N} = f(x). \quad (16)$$

The eigenvalue problem for the $N \times N$ real symmetric matrix \mathbf{H} ,

$$\sum_{m=0}^{N-1} H_{nm} \phi_m(\varepsilon_k) = \varepsilon_k \phi_n(\varepsilon_k), \quad n = 0, \dots, N-1,$$

can be written as

$$\phi_{n+1}(\varepsilon_k) + \frac{J_{n-1}}{J_n} \phi_{n-1}(\varepsilon_k) = 2\xi_n(\varepsilon_k) \phi_n(\varepsilon_k), \quad \xi_n(\varepsilon_k) := \frac{\varepsilon_k - B_n}{2J_n}, \quad (17)$$

subject to Dirichlet boundary conditions $\phi_{-1}(\varepsilon_k) = \phi_N(\varepsilon_k) = 0$. To recast these equations into a more symmetric form, we begin by defining the new unknown vector

$$\psi_n(\varepsilon_k) := \sqrt{J_n} \phi_n(\varepsilon_k)$$

in terms of which (17) becomes

$$\psi_{n+1} + \frac{\sqrt{J_{n+1} J_{n-1}}}{J_n} \psi_{n-1} = 2\sqrt{\frac{J_{n+1}}{J_n}} \xi_n \psi_n \quad (18)$$

(dropping, for simplicity, the ε_k label for the time being). The continuum limit of this equation is obtained by setting

$$\psi_n \rightarrow \psi(x), \quad \psi_{n\pm 1} \rightarrow \psi(x \pm a),$$

and similarly for $\xi_n, J_n, J_{n\pm 1}$:

$$\psi(x+a) + \frac{\sqrt{J(x+a)J(x-a)}}{J(x)} \psi(x-a) = 2\sqrt{\frac{J(x+a)}{J(x)}} \xi(x) \psi(x). \quad (19)$$

Noting that

$$\frac{\sqrt{J(x+a)J(x-a)}}{J(x)} = \left[\left(1 + a \frac{J'(x)}{J(x)} + O(a^2) \right) \left(1 - a \frac{J'(x)}{J(x)} + O(a^2) \right) \right]^{1/2} = 1 + O(a^2),$$

$$\sqrt{\frac{J(x+a)}{J(x)}} = \left(1 + a \frac{J'(x)}{J(x)} + O(a^2) \right)^{1/2} = 1 + a \frac{J'(x)}{2J(x)} + O(a^2),$$

where the prime denotes derivatives with respect to the spatial coordinate x , we can rewrite eq. (19) as

$$\psi(x+a) + \psi(x-a) = 2 \left(1 + a \frac{J'(x)}{2J(x)} \right) \xi(x) \psi(x) + O(a^2). \quad (20)$$

Motivated by the existence of an arbitrarily small length scale—the lattice spacing a —and the highly oscillatory character of typical solutions, we propose the following WKB-type ansatz [22] for the solutions of the previous equation:

$$\psi(x) = e^{\frac{i}{a}S(x)}, \quad \text{with } S(x) := \sum_{n=0}^{\infty} a^n S_n(x). \quad (21)$$

Taylor expanding the exponent

$$S_n(x \pm a) = \sum_{m=0}^{\infty} \frac{(\pm a)^m}{m!} S_n^{(m)}(x)$$

and substituting into the first eq. (21) we arrive at

$$\psi(x \pm a) = \exp \left[\frac{i}{a} S_0(x) + i(S_1(x) \pm S'_0(x)) + ia \left(\frac{1}{2} S''_0(x) \pm S'_1(x) + S_2(x) \right) + O(a^2) \right]. \quad (22)$$

Inserting these expressions into eq. (20) and canceling terms we obtain

$$\exp \left(\frac{ia}{2} S''_0(x) \right) \cos(S'_0(x) + aS'_1(x)) = \left(1 + a \frac{J'(x)}{2J(x)} \right) \xi(x) + O(a^2). \quad (23)$$

We next perform an order by order analysis of the previous equation. At zeroth and first orders we find, respectively,

$$\cos(S'_0(x)) = \xi(x), \quad (24a)$$

$$\frac{i}{2} S''_0(x) \cos(S'_0(x)) - \sin(S'_0(x)) S'_1(x) = \frac{J'(x)}{2J(x)} \xi(x). \quad (24b)$$

These equations have the solution

$$S_0(x, \varepsilon) = \pm \int_0^x ds \arccos \xi(s, \varepsilon) + s_0(\varepsilon), \quad (25a)$$

$$S_1(x, \varepsilon) = -\frac{1}{4i} \log |1 - \xi(x, \varepsilon)^2| \mp \frac{1}{2} \int_0^x dx \frac{\xi(x, \varepsilon)}{\sqrt{1 - \xi(x, \varepsilon)^2}} \frac{J'(x)}{J(x)} + s_1(\varepsilon), \quad (25b)$$

where we have restored the dependency on the energy eigenvalue (represented by the continuous variable ε in the thermodynamic limit). Dropping the irrelevant overall phase $s_0(\varepsilon)/a + s_1(\varepsilon)$, our approximate wave functions thus read

$$\phi(x, \varepsilon) = \frac{A(\varepsilon)}{\sqrt{J(x)|1 - \xi(x, \varepsilon)^2|^{1/2}}} e^{i\varphi(x, \varepsilon)}, \quad (26a)$$

where $A(\varepsilon)$ is a normalization constant (which can be taken as positive without loss of generality) and

$$\varphi(x, \varepsilon) = \int_0^x \frac{ds}{a} \arccos \xi(s, \varepsilon) + O(a^0). \quad (26b)$$

In fact, the \arccos function is multivalued, i.e.,

$$\arccos z = \pm \text{Arccos } z + 2m\pi, \quad m \in \mathbb{Z},$$

where Arccos denotes a particular determination of the inverse cosine. For real z , we shall take

$$\text{Arccos } z = \begin{cases} \pi + i \operatorname{arccosh} |z|, & z < -1, \\ \arccos z, & |z| \leq 1, \\ i \operatorname{arccosh} z, & z > 1, \end{cases}$$

where in the second line $\arccos : [-1, 1] \rightarrow [0, \pi]$ is the standard (real) determination. (For $x < -1$, this determination differs from the principal one [23] in the sign of the imaginary part.) Separating the real and imaginary parts of Arccos we have

$$\text{Arccos } \xi(x, \varepsilon) = \arccos \xi^*(x, \varepsilon) + i\Theta(\xi(x, \varepsilon)^2 - 1) \operatorname{arccosh} |\xi(x, \varepsilon)|,$$

where $\Theta(s) = (1 + \operatorname{sgn} s)/2$ is the Heaviside function and

$$\xi^*(x, \varepsilon) := \begin{cases} -1, & \varepsilon \leq B(x) - 2J(x), \\ \xi(x, \varepsilon) \equiv \frac{\varepsilon - B(x)}{2J(x)}, & B(x) - 2J(x) < \varepsilon < B(x) + 2J(x), \\ 1, & \varepsilon \geq B(x) + 2J(x). \end{cases} \quad (27)$$

Taking $m = 0$ we can therefore express our approximate wave function as

$$\phi(x, \varepsilon) = \frac{A(\varepsilon) e^{\pm \mu(x, \varepsilon)}}{\sqrt{J(x) |1 - \xi(x, \varepsilon)^2|^{1/2}}} e^{\pm i\varphi^*(x, \varepsilon)}, \quad (28a)$$

where the \pm signs in the exponents are correlated, the phase φ^* is given by

$$\varphi^*(x, \varepsilon) := \int_0^x \frac{ds}{a} \arccos \xi^*(s, \varepsilon) + O(a^0), \quad (28b)$$

and

$$\mu(x, \varepsilon) = \int_0^x \frac{ds}{a} \Theta(\xi(s, \varepsilon)^2 - 1) \operatorname{arccosh} |\xi(s, \varepsilon)| + O(a^0)$$

is real and non-negative. It is important, however, to observe that ϕ is defined up to the overall, position-dependent phase

$$\theta_m(x) = \frac{2m\pi x}{a}, \quad m \in \mathbb{Z}. \quad (29)$$

This ambiguity is unavoidable, since this phase is trivial at the chain's sites $x = na$ (with $n = 0, 1, \dots, N-1$), and it will be taken into account in the sequel.

As expected for WKB wave functions, our approximate solution (28a) diverges at the *turning points* determined by the condition $\xi(x, \varepsilon) = \pm 1$, or equivalently

$$\varepsilon = B(x) \pm 2J(x).$$

We then have disconnected WKB solutions in each oscillatory/exponential region, respectively determined by the conditions $|\xi(x, \varepsilon)| < 1$ or $|\xi(x, \varepsilon)| > 1$, i.e.,

$$B(x) - 2J(x) < \varepsilon < B(x) + 2J(x) \quad \text{or} \quad |\varepsilon - B(x)| > 2J(x).$$

The problem is therefore that of finding appropriate connection formulas for these different regions (the analogues of potential wells/barriers in the standard WKB solution method).

More precisely, suppose that for a given value of ε the oscillatory region consists of $g(\varepsilon)$ disjoint intervals (henceforth referred to as *wells*) $I_i(\varepsilon)$, with $i = 1, \dots, g(\varepsilon)$. Since μ is constant inside each of these intervals, and the solution of (17) with a real initial condition ϕ_0 is necessarily real, we can take

$$\phi(x, \varepsilon) = \frac{A_i(\varepsilon) \sin \varphi^*(x, \varepsilon)}{\sqrt{J(x)(1 - \xi(x, \varepsilon)^2)^{1/2}}}, \quad x \in I_i(\varepsilon), \quad (30)$$

with $A_i(\varepsilon)$ a real constant. Note that the choice of cosine or sine (or a linear combination thereof) in the previous formula is purely conventional, since we can absorb an energy dependent constant phase in the $O(a^0)$ term in the phase $\varphi^*(x, \varepsilon)$ (cf. eq. (28b)). We have, however, chosen sine over cosine guided by the behavior of the eigenfunctions in the homogeneous case (cf. section 5). At any rate, we shall see in the next section that this choice is of no consequence for the purposes of approximating the local fermion density, which depends on $\phi(x, \varepsilon)^2$, due to the highly oscillating nature of this term.

Similarly, if the exponential region $\xi(x, \varepsilon) > 1$ consists of a finite number of disjoint intervals $J_j(\varepsilon)$, inside each of these intervals the solution is given by

$$\phi(x, \varepsilon) = \frac{b_j(\varepsilon) e^{\mu(x, \varepsilon)} + c_j(\varepsilon) e^{-\mu(x, \varepsilon)}}{\sqrt{J(x)(\xi(x, \varepsilon)^2 - 1)^{1/2}}}, \quad x \in J_j(\varepsilon),$$

with $b_j(\varepsilon), c_j(\varepsilon)$ real. Indeed, in each of these intervals the phase $\varphi^*(x, \varepsilon)$ is constant, and can therefore be discarded. Note that, since $\mu(x, \varepsilon)$ is clearly positive by its very definition, the term $e^{\mu(x, \varepsilon)}$ is exponentially large and the term $e^{-\mu(x, \varepsilon)}$ exponentially vanishing as $a \rightarrow 0$.

Finally, if the exponential region with $\xi(x, \varepsilon) < -1$ is the disjoint union of a finite number of intervals $\tilde{J}_j(\varepsilon)$, inside each of these intervals the real solution can be taken as

$$\phi(x, \varepsilon) = \frac{\tilde{b}_j(\varepsilon) e^{\mu(x, \varepsilon)} + \tilde{c}_j(\varepsilon) e^{-\mu(x, \varepsilon)}}{\sqrt{J(x)(\xi(x, \varepsilon)^2 - 1)^{1/2}}} \sin \varphi^*(x, \varepsilon), \quad x \in \tilde{J}_j(\varepsilon), \quad (31)$$

with $\tilde{b}_j(\varepsilon), \tilde{c}_j(\varepsilon)$ real. Indeed, now the phase φ^* is *not* constant on $\tilde{J}_j(\varepsilon)$, and thus *cannot* be removed. However, as $\pi \rightarrow -\pi$ under $\varphi^* \rightarrow \varphi^* + \theta_{-1}$, we can regard the sign of the phase $\pm \varphi^*(x, \varepsilon)$ in each of these intervals as independent of the sign of the exponent $\pm \mu(x, \varepsilon)$, up to an irrelevant overall constant phase. (Again, the choice of sine or cosine—or a linear combination thereof—in eq. (31) is largely a matter of convenience.)

Although connection formulas for the coefficients A_i, b_j, c_j , (or \tilde{b}_j, \tilde{c}_j) are relatively straightforward to work out [22], especially if (as is the case in practice) $g(\varepsilon)$ is small, for our purposes it suffices to note that (much as is the case in the ordinary WKB method) for $a \rightarrow 0$ the coefficients $b_j(\varepsilon)$ (or $\tilde{b}_j(\varepsilon)$) of the exponentially growing terms in the ‘forbidden’ region $|x, \varepsilon| > 1$ become exponentially small relative to the corresponding coefficients $c_j(\varepsilon)$ (or $\tilde{c}_j(\varepsilon)$). Thus, *for all practical purposes the WKB solution $\phi(x, \varepsilon)$ can be taken as zero in the region $|\xi(x, \varepsilon)| > 1$* . As we shall show in the next section, this is, in essence, the underlying cause of the depletion/saturation phenomenon that we seek to explain quantitatively.

Remark 3.1. By the previous observations, as $a \rightarrow 0$ the wave function should be supported in the region $|\xi(x, \varepsilon)| \leq 1$, i.e., $B(x) - 2J(x) \leq \varepsilon \leq B(x) + 2J(x)$. For self-consistency, this region should be non-empty for (almost) all single-particle energies ε . Therefore the inequalities

$$\min(B(x) - 2J(x)) \leq \varepsilon \leq \max(B(x) + 2J(x)) \quad (32)$$

should provide a heuristic estimate of the range of the single-particle spectrum. In fact, Gershgorin's Circle Theorem [24] for the eigenvalues of a general (complex) matrix applied to \mathbf{H} yields the *exact* bounds

$$\min(B_n - J_n - J_{n-1}) \leq \varepsilon_k \leq \max(B_n + J_n + J_{n-1}),$$

whose continuum limit is eq. (32). Furthermore, when $B_n = B$ and $J_n = J$ for all n the minimum/maximum single-particle energies are respectively $\varepsilon_0 = B - 2J$, $\varepsilon_{N-1} = B + 2J$. This suggests that when B_n and J_n vary slowly we should have

$$\varepsilon_0 \underset{N \gg 1}{\simeq} \min(B(x) - 2J(x)), \quad \varepsilon_{N-1} \underset{N \gg 1}{\simeq} \max(B(x) + 2J(x)). \quad (33)$$

Our numerical simulations do indeed confirm this surmise. \square

If we set to zero the wave function in the region $|\xi(x, \varepsilon)| > 1$ (which, as remarked above, should be an excellent approximation in the limit $a \rightarrow 0$), the WKB wave function $\phi(x, \varepsilon)$ will be given by the sum of the $g(\varepsilon)$ localized, non-overlapping functions

$$\phi_i(x, \varepsilon) = \frac{A_i(\varepsilon) \sin \varphi^*(x, \varepsilon)}{\sqrt{J(x)(1 - \xi(x, \varepsilon)^2)^{1/2}}} \chi_i(x) =: A_i(\varepsilon) f_i(x, \varepsilon), \quad i = 1, \dots, g(\varepsilon), \quad (34)$$

where $\chi_i(x) := \chi_{I_i(\varepsilon)}(x)$ is the characteristic function of the interval $I_i(\varepsilon)$. In practice, unless the 'profile' $\xi(x, \varepsilon)$ (which depends on J_n , B_n , and ε) is symmetric about the chain's midpoint, or the energy ε is such that the separation between consecutive wells is negligible, the eigenfunction of \mathbf{H} of energy (close to) ε will be localized on a single interval roughly coinciding with one of the wells $I_i(\varepsilon)$. Thus typically the single-particle eigenfunctions will be described by a WKB wave function of the form (34) for a *single* appropriate i , which in general depends on the energy ε . In fact, for many chains of interest—including the Krawtchouk and rainbow chains discussed in section (5), and the Rindler chain examined in the Supplementary Material—the profile $\xi(x, \varepsilon)$ determines only a single well. In this case eq. (34) simplifies to

$$\phi(x, \varepsilon) = \frac{A(\varepsilon) \sin \varphi^*(x, \varepsilon)}{\sqrt{J(x)(1 - \xi(x, \varepsilon)^2)^{1/2}}} \Theta(1 - \xi(x, \varepsilon)^2), \quad (35a)$$

where $A(\varepsilon) > 0$ is a normalization constant. As $a \rightarrow 0$, the normalization constant $A(\varepsilon)$ can be approximated with increasing accuracy by averaging $\sin^2(\varphi^*(x, \varepsilon))$ over distances of the order of a , with the result

$$A(\varepsilon)^{-2} = \int_0^\ell dx \frac{\Theta(1 - \xi(x, \varepsilon)^2)}{2J(x)\sqrt{1 - \xi(x, \varepsilon)^2}}. \quad (35b)$$

We shall see in section 5 that the approximation (35) yields a formula for the fermionic density which is in excellent agreement with the numerical results. It also follows from this equation that the envelopes of the WKB wave function $\phi(x, \varepsilon)$ are in this case the two curves

$$y = \pm \frac{A(\varepsilon) \Theta(1 - \xi(x, \varepsilon)^2)}{\sqrt{J(x)(1 - \xi(x, \varepsilon)^2)^{1/2}}}. \quad (36)$$

Remark 3.2. In the absence of an external magnetic field, the spectrum of the chain (2) is symmetric about zero. Moreover, it can be shown (see, e.g., [16]) that the single-particle wave functions with energies ε_k and $-\varepsilon_k$ are related by

$$\phi_n(-\varepsilon_k) = (-1)^n \phi_n(\varepsilon_k) \quad (37)$$

(up to an overall sign). It is straightforward to check that the WKB approximate wave functions (35a) share this symmetry. Indeed, if $B(x) = 0$ for all x we have $\xi^*(x, -\varepsilon) = -\xi^*(x, \varepsilon)$, and hence

$$a\varphi^*(x, -\varepsilon) = \int_0^x ds \arccos \xi^*(x, -\varepsilon) = \int_0^x ds (\pi - \arccos \xi^*(x, \varepsilon)) = \pi x - a\varphi^*(x, \varepsilon).$$

We can thus write

$$\phi(x, -\varepsilon) = \frac{A(\varepsilon) \sin\left(\frac{\pi x}{a} - \varphi^*(x, \varepsilon)\right)}{\sqrt{J(x)(1 - \xi(x, \varepsilon)^2)^{1/2}}} \Theta(1 - \xi(x, \varepsilon)^2),$$

since $\xi(x, -\varepsilon)^2 = \xi(x, \varepsilon)^2$ when $B = 0$ and $A(-\varepsilon) = A(\varepsilon)$ on account of eq. (35b). In particular, on lattice sites $x = na$ we have

$$\phi(na, -\varepsilon) = (-1)^{n+1} \phi(na, \varepsilon), \quad (38)$$

which is essentially eq. (37). Obviously, a similar remark can be made for the “localized” WKB eigenfunctions $\phi_i(x, \varepsilon)$ in eq. (34). \square

4 Fermionic density profile

As mentioned in section 2, the single-particle Hamiltonian matrix \mathbf{H} and its corresponding wave functions are related to a finite family of monic orthogonal polynomials $\{P_n(\varepsilon)\}_{n=0}^N$ (see, e.g., ref. [10]). Indeed, \mathbf{H} is precisely the Jacobi matrix associated to this polynomial family, and thus its spectrum consists of the roots of the polynomial P_N or, in the thermodynamic limit, of the function $\phi(\ell, \varepsilon)$. This condition is also a direct consequence of the fact that we have imposed Dirichlet boundary conditions in the recursion relation (17). Therefore in the thermodynamic limit the single-particle energies should satisfy the condition $\phi(\ell, \varepsilon) = 0$. We shall next use this condition to derive a closed-form asymptotic approximation to the single-fermion density of states $D(\varepsilon)$.

Let us suppose, to begin with, that the WKB approximation to eigenfunctions with energies in the range $[\varepsilon, \varepsilon + d\varepsilon]$ is supported on a single interval, and is thus given by eq. (35a). If the endpoint $x = \ell$ falls on the region $|\xi(x, \varepsilon)| \leq 1$, by eq. (30) we must have

$$\varphi^*(\ell, \varepsilon) = n\pi, \quad \text{with } n \in \mathbb{Z}. \quad (39)$$

It may naively seem that the boundary condition (39) becomes vacuous when the endpoint $x = \ell$ falls on a depletion/saturation region $|\xi(x, \varepsilon)| > 1$. To see that this is actually not the case, let us denote the non-depletion interval $|\xi(x, \varepsilon)| < 1$ by $I(\varepsilon) = (x_1(\varepsilon), x_2(\varepsilon))$, with $x_2(\varepsilon) < \ell$. The continuity of the wave function at $x = x_2(\varepsilon)$ then requires that $\phi(x_2(\varepsilon), \varepsilon) = 0$, or equivalently that

$$\varphi^*(x_2(\varepsilon), \varepsilon) = k\pi, \quad \text{with } k \in \mathbb{Z}. \quad (40)$$

Suppose, first, that $\xi(\ell, \varepsilon) > 1$, and hence $\xi > 1$ on $[x_2(\varepsilon), \ell]$. Since in this case the phase φ^* is constant on the interval $[x_2(\varepsilon), \ell]$, eq. (40) implies (39). Suppose, next, that $\xi(\ell, \varepsilon) < -1$,

and thus $\xi < -1$ on $[x_2(\varepsilon), \ell]$. Since now $\xi^* = \pi$ on the interval $[x_2(\varepsilon), \ell]$, by eq. (28b) we have

$$\varphi^*(x, \varepsilon) = \varphi^*(x_2(\varepsilon), \varepsilon) + \frac{\pi}{a} (x - x_2(\varepsilon)) = k\pi + \frac{\pi}{a} (x - x_2(\varepsilon)), \quad x_2(\varepsilon) \leq x \leq \ell(\varepsilon),$$

with $k \in \mathbb{Z}$. However, we can change the sign of the last term in the previous equation by adding θ_{-1} to φ^* , with the result

$$\varphi^*(x, \varepsilon) = k\pi - \frac{\pi}{a} (x - x_2(\varepsilon)), \quad x_2(\varepsilon) \leq x \leq \ell(\varepsilon).$$

Since the phase must be unambiguous at the lattice site $x = \ell$, we must have

$$\frac{2\pi}{a} (\ell - x_2(\varepsilon)) = 2m\pi$$

for some integer m . Hence

$$\varphi^*(\ell, \varepsilon) = (k + m)\pi,$$

which is again eq. (39).

By eq. (39), any two contiguous energy levels must satisfy

$$|\varphi^*(\ell, \varepsilon_{k+1}) - \varphi^*(\ell, \varepsilon_k)| = \pi.$$

Since the single-particle energy spectrum becomes approximately continuous as $a \rightarrow 0$, we can define an arbitrarily small level spacing $\Delta\varepsilon_k := \varepsilon_{k+1} - \varepsilon_k$. From the previous equation we then deduce that

$$\pi = |\partial_\varepsilon \varphi^*(\ell, \varepsilon_k)| \Delta\varepsilon_k + O((\Delta\varepsilon_k)^2).$$

On the other hand, from eq. (28b) for the phase φ^* we obtain

$$\partial_\varepsilon \varphi^*(\ell, \varepsilon) = \int_0^\ell \frac{dx}{a} \partial_\varepsilon \arccos \xi^*(x, \varepsilon) + O(a^0), \quad (41)$$

since $\xi^*(x, \varepsilon)$ is continuous by construction. Taking into account that $\xi^*(x, \varepsilon)$ is constant in the region where $|\xi(x, \varepsilon)| > 1$ we then obtain

$$\partial_\varepsilon \varphi^*(\ell, \varepsilon) = - \int_0^\ell \frac{dx}{a} \frac{\Theta(1 - \xi(x, \varepsilon)^2)}{2J(x)\sqrt{1 - \xi(x, \varepsilon)^2}} + O(a^0) = - \frac{A(\varepsilon)^{-2}}{a} + O(a^0),$$

with $A(\varepsilon)$ defined in eq. (35b). Therefore in the continuum limit $\Delta\varepsilon_k \rightarrow \Delta(\varepsilon)$, with

$$\Delta(\varepsilon) = \frac{\pi}{|\partial_\varepsilon \varphi^*(\ell, \varepsilon)|} = \pi a A(\varepsilon)^2 + O(a^2). \quad (42)$$

This result immediately yields the single-fermion density of states

$$D(\varepsilon) = \frac{1}{\Delta(\varepsilon)} = \frac{A(\varepsilon)^{-2}}{\pi a} = \frac{1}{2\pi a} \int_0^\ell dx \frac{\Theta(1 - \xi(x, \varepsilon)^2)}{J(x)\sqrt{1 - \xi(x, \varepsilon)^2}}, \quad (43)$$

where (as we shall do in the sequel) we have discarded the subleading term $O(a^0)$.

Suppose, next, that for energies in the range $[\varepsilon, \varepsilon + d\varepsilon]$ the region $|\xi(x, \varepsilon)| \leq 1$ consists of $g(\varepsilon) > 1$ wells $I_i(\varepsilon)$. Let us also assume that, as is almost always the case in practice, the eigenfunctions of \mathbf{H} with energies in this range are supported within a single well. Let $D_i(\varepsilon)d\varepsilon$ denote the number of eigenfunctions with energies in the range $[\varepsilon, \varepsilon + d\varepsilon]$ supported on the well $I_i(\varepsilon)$. By a slight modification of the previous argument (essentially, redefining $\xi^*(x, \varepsilon)$)

so that it is constant outside the interval $I_i(\varepsilon)$ and still continuous), we easily arrive at the formula

$$D_i(\varepsilon) = \frac{A_i(\varepsilon)^{-2}}{\pi a}, \quad (44a)$$

with

$$A_i(\varepsilon)^{-2} = \int_0^\ell \frac{\chi_i(x) dx}{2J(x)\sqrt{1-\xi(x,\varepsilon)^2}} = \int_{I_i(\varepsilon)} \frac{dx}{2J(x)\sqrt{1-\xi(x,\varepsilon)^2}}. \quad (44b)$$

Hence in this case the total single-particle density of states is given by the sum

$$D(\varepsilon) = \sum_{i=1}^{g(\varepsilon)} D_i(\varepsilon) = \frac{1}{\pi a} \sum_{i=1}^{g(\varepsilon)} A_i(\varepsilon)^{-2}. \quad (45)$$

We shall assume that the previous formula is valid in all generality (i.e., also in the rare cases in which there are eigenfunctions of \mathbf{H} supported in several disjoint wells). As we shall see in the sequel, this assumption is fully supported by the accuracy of the approximations to the fermion density and the filling fraction in all the examples presented in section 5.

With the help of the general formula (45) we can now determine an important property related to energy, namely the mode filling fraction. Indeed, for a given total occupation M corresponding to a Fermi energy $\varepsilon_F = \varepsilon_{M-1}$, we may calculate the filling fraction ν as

$$\nu(\varepsilon_F) = \frac{1}{N} \sum_{k=0}^{M-1} 1 \rightarrow \frac{a}{\ell} \int_{\varepsilon_0}^{\varepsilon_F} d\varepsilon D(\varepsilon).$$

We thus obtain

$$\begin{aligned} \nu(\varepsilon_F) &= \frac{1}{2\pi\ell} \int_{\varepsilon_0}^{\varepsilon_F} d\varepsilon \sum_{i=1}^{g(\varepsilon)} \int_0^\ell \frac{\chi_i(x) dx}{J(x)\sqrt{1-\xi(x,\varepsilon)^2}} = \frac{1}{2\pi\ell} \int_{\varepsilon_0}^{\varepsilon_F} d\varepsilon \int_0^\ell dx \frac{\Theta(1-\xi(x,\varepsilon)^2)}{J(x)\sqrt{1-\xi(x,\varepsilon)^2}} \\ &= \frac{1}{\pi\ell} \int_0^\ell dx \int_{-1}^{\xi^*(x,\varepsilon_F)} \frac{d\xi}{\sqrt{1-\xi^2}}, \end{aligned} \quad (46)$$

where we have taken into account that $\xi(x, \varepsilon_0) = -1$ by eq. (33). Evaluating the innermost integral we obtain

$$\nu(\varepsilon_F) = \frac{1}{\pi\ell} \int_0^\ell dx \arccos(-\xi^*(x, \varepsilon_F)), \quad (47)$$

or equivalently

$$\nu(\varepsilon_F) = 1 - \frac{1}{\pi\ell} \int_0^\ell dx \arccos \xi^*(x, \varepsilon_F) = \frac{1}{2} + \frac{1}{\pi\ell} \int_0^\ell dx \arcsin \xi^*(x, \varepsilon_F),$$

which are sometimes more convenient forms. Inverting any of these expressions, when possible, yields the Fermi energy as a function of the filling fraction.

Remark 4.1. The previous analysis predicts that when the set $\{x \in [0, \ell] : |\xi(x, \varepsilon)| \leq 1\}$ consists of $g(\varepsilon)$ disjoint intervals (wells) $I_i(\varepsilon)$, and each single-particle eigenfunction with energy near ε is localized within one of these wells, the relative frequency of eigenfunctions localized in the well $I_i(\varepsilon)$ is given by $A(\varepsilon)^2/A_i(\varepsilon)^2$. This prediction is fully supported by our numerical results. For instance, in fig. 1 we present a plot of the single-particle eigenfunctions of the general cosine chain (79) with $N = 400$ spins and energies $\varepsilon_{\frac{N}{2}+i}$ for $i = -20, -19, \dots, 19$, each of which is supported on one of three intervals I_1 (left end), I_2 (middle), and I_3 (right end). As can be seen from the figure, the number of eigenfunctions supported on each of these

wells are respectively 8, 22, and 10. The corresponding frequencies 0.2, 0.55, and 0.25 are remarkably close to the WKB predictions

$$\frac{A(\varepsilon_{N/2})^2}{A_1(\varepsilon_{N/2})^2} = 0.211558, \quad \frac{A(\varepsilon_{N/2})^2}{A_2(\varepsilon_{N/2})^2} = 0.547223, \quad \frac{A(\varepsilon_{N/2})^2}{A_3(\varepsilon_{N/2})^2} = 0.241218. \quad \square$$

Remark 4.2. By eq.(43) and the second equality in eq.(46), the asymptotic formula (47) coincides with the result that would be obtained by assuming that, for any energy ε , eq. (35a) is the WKB approximation to the exact single-particle eigenfunction at that energy. Of course, we know that this is only the case when there is only one well for every single-particle energy ε . In the general case in which the region $|\xi(x, \varepsilon)| \leq 1$ consists of $g(\varepsilon)$ wells, by eq. (34) we can express the WKB wave function (35a) as

$$\phi(x, \varepsilon) = \frac{A(\varepsilon) \sin \varphi^*(x, \varepsilon)}{\sqrt{J(x)(1 - \xi(x, \varepsilon)^2)^{1/2}}} \sum_{i=1}^{g(\varepsilon)} \chi_i(x) = \sum_{i=1}^{g(\varepsilon)} \frac{A(\varepsilon)}{A_i(\varepsilon)} \phi_i(x, \varepsilon). \quad (48)$$

In other words, in general $\phi(x, \varepsilon)$ is not an approximation to a true eigenfunction, but rather a linear combination with weights proportional to $A_i(\varepsilon)^{-1}$ of the single-particle approximate WKB eigenfunctions ϕ_i supported on each of the wells $I_i(\varepsilon)$. Note also that, since both ϕ and each ϕ_i are normalized, and $\phi_i(x, \varepsilon)$ does not overlap with $\phi_j(x, \varepsilon)$ for $j \neq i$, from eq. (48) we have

$$A(\varepsilon)^{-2} = \sum_{i=1}^{g(\varepsilon)} A_i(\varepsilon)^{-2}.$$

In particular, when by reasons of symmetry all the normalization constants $A_i(\varepsilon)$ are equal, from the previous equations we obtain

$$\phi(x, \varepsilon) = \frac{1}{\sqrt{g(\varepsilon)}} \sum_{i=1}^{g(\varepsilon)} \phi_i(x, \varepsilon). \quad \square$$

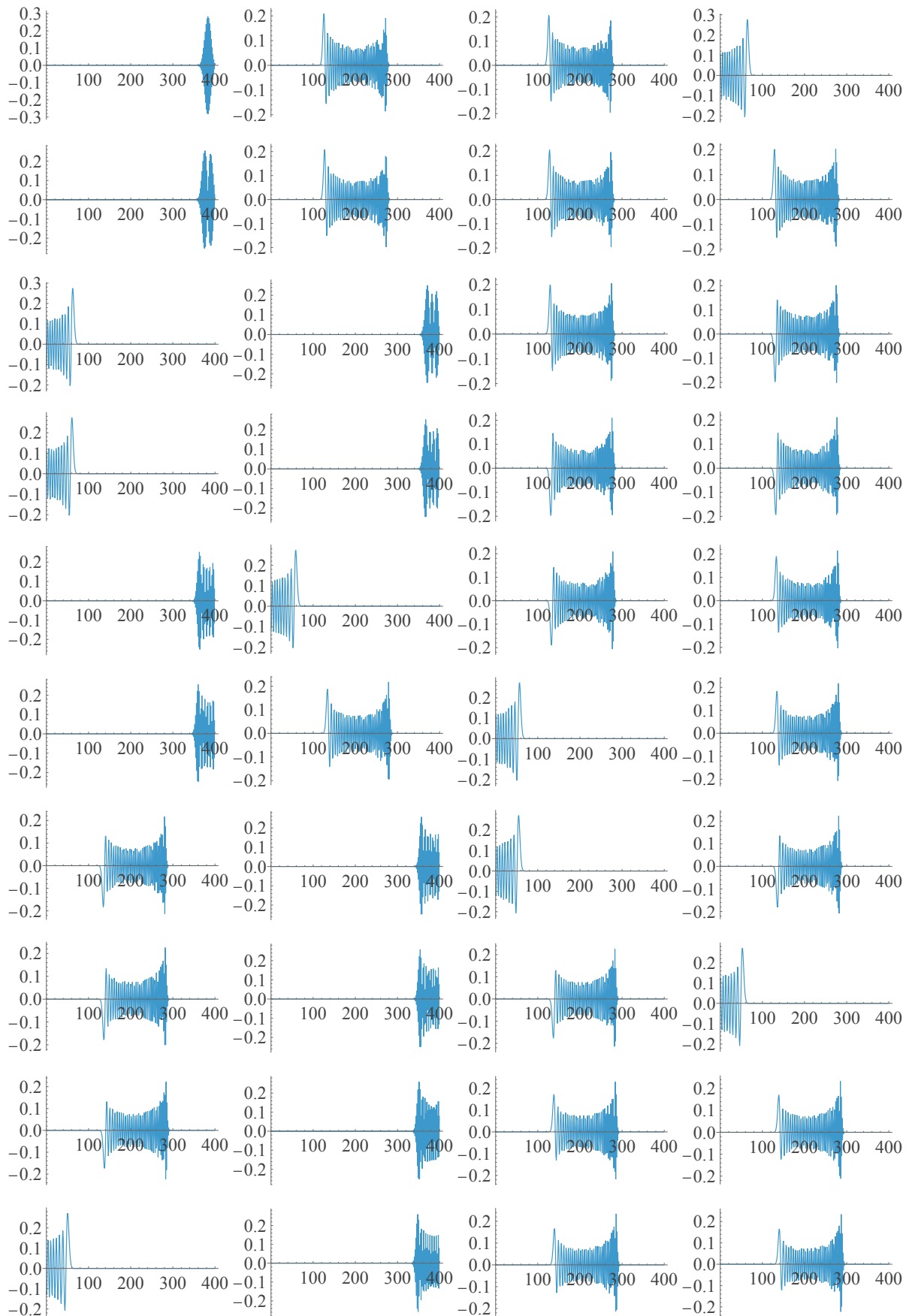


Figure 1: Eigenfunctions of the general cosine chain (79) with $N = 400$ spins and energies $\varepsilon_{\frac{N}{2}+i}$ for $i = -20, -19, \dots, 19$ (from top to bottom and left to right).

We next derive an asymptotic approximation to the fermionic density (per unit length)

$$\rho(x, \varepsilon_F) := \frac{1}{a} \langle M | c_{x/a}^\dagger c_{x/a} | M \rangle,$$

where $|M\rangle$ is the state (11) filled with single-particle modes with energies $\varepsilon \leq \varepsilon_F$. We can approximate $\rho(x, \varepsilon_F)$ by replacing the sum in eq. (14) by an integral, with the result⁴

$$\rho(x, \varepsilon_F) = \int_{\varepsilon_0}^{\varepsilon_F} d\varepsilon \sum_{i=1}^{g(\varepsilon)} D_i(\varepsilon) \phi_i(x, \varepsilon)^2 = \frac{1}{\pi a} \int_{\varepsilon_0}^{\varepsilon_F} d\varepsilon \sum_{i=1}^{g(\varepsilon)} \frac{\phi_i(x, \varepsilon)^2}{A_i(\varepsilon)^2}, \quad (49)$$

where we have used eq. (44). From eq. (34) we then obtain

$$\begin{aligned} \rho(x, \varepsilon_F) &= \frac{1}{\pi a} \int_{\varepsilon_0}^{\varepsilon_F} d\varepsilon \frac{\sin^2 \varphi^*(x, \varepsilon)}{J(x) \sqrt{1 - \xi(x, \varepsilon)^2}} \sum_{i=1}^{g(\varepsilon)} \chi_i(x) \\ &= \frac{1}{\pi a} \int_{\varepsilon_0}^{\varepsilon_F} d\varepsilon \frac{\sin^2 \varphi^*(x, \varepsilon)}{J(x) \sqrt{1 - \xi(x, \varepsilon)^2}} \Theta(1 - \xi(x, \varepsilon)^2). \end{aligned}$$

Averaging $\sin^2 \varphi^*(x, \varepsilon)$ over a distance of order a we finally obtain the asymptotic formula

$$\rho(x, \varepsilon_F) = \frac{1}{2\pi a} \int_{\varepsilon_0}^{\varepsilon_F} d\varepsilon \frac{\Theta(1 - \xi(x, \varepsilon)^2)}{J(x) \sqrt{1 - \xi(x, \varepsilon)^2}} = \frac{1}{\pi a} \int_{-1}^{\xi^*(x, \varepsilon_F)} \frac{d\xi}{\sqrt{1 - \xi^2}},$$

and therefore

$$\rho(x, \varepsilon_F) = \frac{1}{\pi a} \arccos(-\xi^*(x, \varepsilon_F)). \quad (50)$$

This approximate expression for the fermionic density profile—together with its discrete version (5) anticipated in the Introduction—is one of the main results in this work. Equivalent forms of it that we shall sometimes use are

$$a\rho(x, \varepsilon_F) = 1 - \frac{1}{\pi} \arccos \xi^*(x, \varepsilon_F) = \frac{1}{2} + \frac{1}{\pi} \arcsin \xi^*(x, \varepsilon_F).$$

From eq. (50) and the definition (27) of ξ^* it immediately follows that the local fermion density should vanish on the set $\{x \in [0, \ell] : \varepsilon_F \leq B(x) - 2J(x)\}$, while it should saturate to one on the set $\{x \in [0, \ell] : \varepsilon_F \geq B(x) + 2J(x)\}$. The corresponding domains (in general, unions of disjoint intervals) are thus identified as the *depletion* and *saturation* regions of the fermionic density, respectively. It is also worth remarking that eq. (50) is fully consistent with eq. (47), since the mode filling ν can be calculated as

$$\nu(\varepsilon_F) = \frac{1}{N} \int_0^\ell dx \rho(x, \varepsilon_F) = \frac{1}{\ell} \int_0^\ell dx a\rho(x, \varepsilon_F).$$

Note, finally, that at low filling ($\xi^*(x, \varepsilon_F) \gtrsim -1$) we have

$$\rho(x, \varepsilon_F) = \frac{\sqrt{2}}{\pi a} \sqrt{1 + \xi^*(x, \varepsilon_F)} \left[1 + O(1 + \xi^*(x, \varepsilon_F)) \right] \simeq \frac{1}{\pi a} \sqrt{2 + \frac{\varepsilon_F - B(x)}{J(x)}}. \quad (51)$$

In particular, when the magnetic field is identically zero the previous expression reduces to eq. (38) in ref. [17]. It should be stressed, however, that eq. (50) is valid also in the presence of an external magnetic field and, perhaps more importantly, for arbitrary fillings.

⁴We have again taken into account that $\Phi_{nk} \mapsto \sqrt{a} \phi(na, \varepsilon_k)$ as $N \rightarrow \infty$.

Remark 4.3. A popular alternative choice of the free fermionic Hamiltonian (2) is

$$\hat{H} = - \sum_{n=0}^{N-2} \hat{J}_n (c_n^\dagger c_{n+1} + \text{H.c.}) + \sum_{n=0}^{N-1} B_n c_n^\dagger c_n, \quad (52)$$

with $\hat{J}_n > 0$ for all n ; see, e.g., ref. [17]. (Obviously, this is equivalent to taking $J_n < 0$ for all n in eq. (2).) It is straightforward to show that if $\phi_n(\varepsilon)$ is a single-particle eigenfunction of H with energy ε then $\hat{\phi}_n(\varepsilon) = (-1)^n \phi_n(\varepsilon)$ is an eigenfunction of \hat{H} with the same energy. Hence H and \hat{H} have the same single-particle spectrum, and therefore the filling fraction (as a function of the Fermi energy) is identical for both chains. The same is obviously true for the average local occupation $\langle c_n^\dagger c_n \rangle$, since

$$\langle c_n^\dagger c_n \rangle = \sum_{k=0}^{M-1} \phi_n(\varepsilon_k)^2$$

and $\hat{\phi}_n^2 = \phi_n^2$. Thus the Hamiltonians in eqs. (2) and (52) have the same fermionic density profile and, in particular, share the same depletion/saturation regions. As a consequence, the WKB approximations to the filling fraction, the envelopes of the single-particle wave functions, and the fermionic density obtained in this and the previous section are valid for the fermionic chain (52) as well, provided that we replace $J(x)$ by $\hat{J}(x)$. \square

Remark 4.4. When $B(x)$ vanishes identically we obviously have $\xi(x, -\varepsilon) = -\xi(x, \varepsilon)$, and therefore $\xi(x, -\varepsilon) \gtrless \pm 1$ if and only if $\xi(x, \varepsilon) \lessgtr \mp 1$. It follows that

$$\arccos(-\xi^*(x, -\varepsilon)) = \pi - \arccos(-\xi^*(x, \varepsilon)),$$

and hence

$$a\rho(x, -\varepsilon_F) = 1 - a\rho(x, \varepsilon_F), \quad \nu(-\varepsilon_F) = 1 - \nu(\varepsilon_F). \quad (53)$$

Thus our approximate formula (50) for the fermionic density is consistent with the particle-hole symmetry that occurs when $B(x)$ is identically zero. Of course, this property could have also been established directly from eq. (38) for the WKB wave functions. If, in addition, $\varepsilon_F = 0$ (i.e., at half filling) it follows from the previous equation that $a\rho(x, 0) = 1/2$. We thus recover the well-known result that the fermionic density is constant at half-filling and zero magnetic field. \square

Equation (50) allows us to deduce interesting global properties of the fermionic density that are difficult to predict a priori, in particular regarding the influence of the magnetic field on the depletion/saturation phenomenon. For example, in the absence of an external magnetic field the depletion and saturation regions are determined by the equations $\varepsilon_F \leq -2J(x)$ and $\varepsilon_F \geq 2J(x)$, respectively. Thus there are no depletion and saturation intervals for Fermi energies $\varepsilon_F \in [-2 \min_{x \in [0, \ell]} J(x), 2 \min_{x \in [0, \ell]} J(x)]$. Moreover, for $\varepsilon_F \in [-2 \max_{x \in [0, \ell]} J(x), -2 \min_{x \in [0, \ell]} J(x)]$ only depletion regions can appear, while for $\varepsilon_F \in [2 \min_{x \in [0, \ell]} J(x), 2 \max_{x \in [0, \ell]} J(x)]$ only saturation intervals may occur.

In the same vein, using eq. (50) it is a straightforward matter to construct chains without depletion or saturation regions for *all* fillings. Indeed, if $J(0) = 0$ and $B(x) = 2J(x)$ by eq. (50) there are no depletion regions and there is at least one saturation region at the left end of the chain (see fig. 2 left). Moreover, if J is monotonically increasing there are no other saturation regions; this is the case, for instance, with the Rindler chain discussed in the Supplementary Material. Similarly, taking $B(x) = -2J(x)$ we obtain a chain with no saturation regions and at least one depletion region at the right end of the chain, with no other such regions if J is monotonic (cf. fig. 2, right panel). (Of course, to construct chains with only depletion or saturation intervals respectively growing from the left or right endpoint, it suffices to take $J(\ell) = 0$ instead of $J(0) = 0$.)

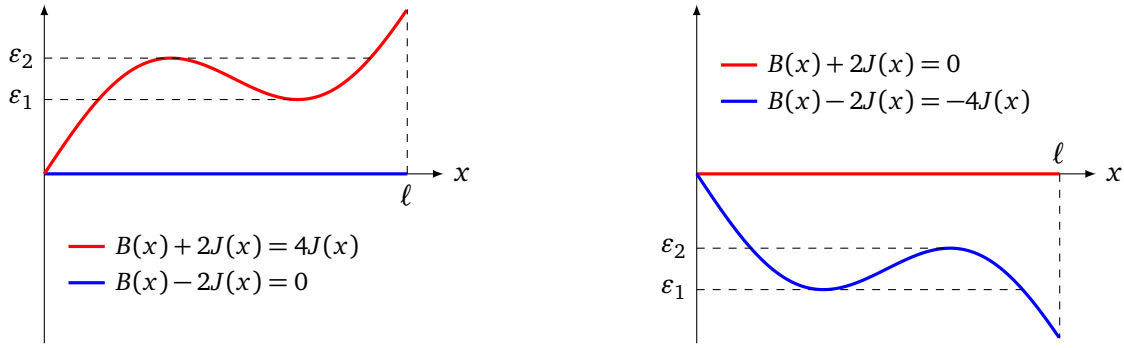


Figure 2: Plots of $B(x) \pm 2J(x)$ for $B(x) = 2J(x)$ (left) and $B(x) = -2J(x)$ (right), for a continuum coupling $J(x)$ vanishing at the origin. In the former case there is a single saturation interval $[0, x_1(\varepsilon_F)]$ for Fermi energies $\varepsilon_F \in [0, \varepsilon_1]$, where $x_1(\varepsilon_F)$ is the smallest positive root of the equation $4J(x) = \varepsilon_F$. A second, disjoint saturation interval $[x_2(\varepsilon_F), x_3(\varepsilon_F)]$ appears when $\varepsilon_F \in (\varepsilon_1, \varepsilon_2)$, where $x_2(\varepsilon_F)$ and $x_3(\varepsilon_F)$ are the second and third smallest positive roots of the equation $4J(x) = \varepsilon_F$. These two saturation regions merge into a single interval $[0, x_1(\varepsilon_F)]$ for energies above ε_2 . The situation is similar for the case $B(x) = -2J(x)$ represented in the right panel, the saturation intervals becoming depletion ones.

5 Examples

5.1 The homogeneous chain

Consider, to begin with, the homogeneous chain with

$$B_n = B, \quad J_n = J$$

for all n . As mentioned in section 3, in this case the single-particle spectrum is known in closed form [25]. More precisely, the single-particle energies (in increasing order) are given by

$$\varepsilon_{k-1} = B - 2J \cos\left(\frac{\pi k}{N+1}\right), \quad k = 1, \dots, N, \quad (54)$$

and their corresponding (normalized) eigenfunctions $\sum_{n=1}^N \Phi_{n-1,k-1} |n-1\rangle$ have components

$$\Phi_{n-1,k-1} = (-1)^{n-1} \sqrt{\frac{2}{N+1}} \sin\left(\frac{\pi n k}{N+1}\right), \quad n, k = 1, \dots, N. \quad (55)$$

In this case

$$\xi(x, \varepsilon) = \frac{\varepsilon - B}{2J} \equiv \xi(\varepsilon)$$

is independent of x , and $|\xi(\varepsilon)| \leq 1$ on account of eq. (54). It follows that $\xi^*(x, \varepsilon) = \xi(\varepsilon)$, and therefore

$$\varphi^*(x, \varepsilon) = \int_0^x \frac{ds}{a} \arccos \xi(\varepsilon) = \frac{x}{a} \arccos \xi(\varepsilon).$$

Moreover, by eq. (35b) we have

$$A(\varepsilon)^{-2} = \frac{\ell}{2J \sqrt{1 - \xi(\varepsilon)^2}},$$

and hence the approximate WKB eigenfunctions in this case reduce to

$$\phi(x, \varepsilon) = \sqrt{\frac{2}{\ell}} \sin\left(\frac{x}{a} \arccos \xi(\varepsilon)\right).$$

On the other hand,

$$\begin{aligned} \sqrt{a} \phi(na, \varepsilon_{k-1}) &= \sqrt{\frac{2}{N}} \sin\left(n \arccos\left(\frac{\varepsilon_{k-1} - B}{2J}\right)\right) = \sqrt{\frac{2}{N}} \sin\left(n \arccos\left(-\cos\left(\frac{\pi k}{N+1}\right)\right)\right) \\ &= \sqrt{\frac{2}{N}} \sin\left(n\pi - \frac{\pi nk}{N+1}\right) = (-1)^{n-1} \sqrt{\frac{2}{N}} \sin\left(\frac{\pi nk}{N+1}\right) \\ &= \sqrt{\frac{N}{N+1}} \Phi_{n-1, k-1}, \end{aligned}$$

so that the relative error in the WKB wave function is $O(N^{-1})$.

By eq. (54), the filling $\nu = M/N$ (with $M = 1, \dots, N$) is in this case given by

$$\nu(\varepsilon_{M-1}) = \frac{N+1}{N\pi} \arccos(-\xi_{M-1}).$$

This should be compared with our approximate formula (47), which in this case (taking $\varepsilon_F = \varepsilon_{M-1}$) reads

$$\nu(\varepsilon_{M-1}) = \frac{1}{\pi\ell} \ell \arccos(-\xi_{M-1}) = \frac{1}{\pi} \arccos(-\xi_{M-1}),$$

with a relative error again of order N^{-1} . Likewise, the level spacing $\Delta\varepsilon_{k-1} = \varepsilon_k - \varepsilon_{k-1}$ can be directly computed from eq. (54), with the result

$$\Delta\varepsilon_{k-1} = 2J \left[\cos\left(\frac{\pi k}{N+1}\right) - \cos\left(\frac{\pi(k+1)}{N+1}\right) \right] \simeq \frac{2\pi J}{N+1} \sin\left(\frac{\pi k}{N+1}\right).$$

On the other hand, its continuous approximation (42) is given by

$$\Delta(\varepsilon) = \pi a A(\varepsilon)^2 = \frac{2\pi J}{N} \sqrt{1 - \xi(\varepsilon)^2},$$

which evaluated at $\varepsilon = \varepsilon_{k-1}$ yields

$$\Delta(\varepsilon_{k-1}) = \frac{2\pi J}{N} \sqrt{1 - \left(\frac{\varepsilon_{k-1} - B}{2J}\right)^2} = \frac{2\pi J}{N} \sin\left(\frac{\pi k}{N+1}\right) = \Delta\varepsilon_{k-1} + O(N^{-1}).$$

Consider, finally, the approximation (50) to the fermionic density, which in this case is simply

$$\rho(x, \varepsilon_F) = \frac{1}{\pi a} \arccos(-\xi(\varepsilon_F)).$$

Taking $\varepsilon_F = \varepsilon_{M-1}$ for a filling fraction $\nu = M/N$ we obtain the WKB approximation (5) to the average number of fermions at site n :

$$\langle c_n^\dagger c_n \rangle \equiv \langle M | c_n^\dagger c_n | M \rangle \approx a \rho(na, \varepsilon_{M-1}) = \frac{1}{\pi} \arccos(-\xi(\varepsilon_{M-1})) = \frac{1}{\pi} \frac{\pi M}{N+1} = \nu + O(N^{-1}).$$

In other words, in the thermodynamic limit the fermionic density should be constant for any filling and magnetic field strength. For finite N , the fermionic density can be exactly computed with the help of the explicit formula (55), namely

$$\langle c_{n-1}^\dagger c_{n-1} \rangle = \frac{2}{N+1} \sum_{k=0}^{M-1} \sin^2\left(\frac{\pi nk}{N+1}\right) = \frac{M}{N+1} - \frac{\sin\left(\frac{M\pi n}{N+1}\right) \cos\left(\frac{(M-1)\pi n}{N+1}\right)}{(N+1) \sin\left(\frac{\pi n}{N+1}\right)}.$$

Thus in the bulk (i.e., for n away from 1 and N) and in the thermodynamic limit the average number of fermions is indeed independent of the site—and, as a consequence, simply equal to the filling fraction ν . As expected, $\langle c_{n-1}^\dagger c_{n-1} \rangle$ features characteristic Friedel oscillations [26] near the chain's ends. For example, for small $n \geq 1$ we have

$$\langle c_{n-1}^\dagger c_{n-1} \rangle \approx \frac{M}{N+1} - \frac{\sin\left(\frac{2M\pi n}{N+1}\right)}{2\pi n},$$

which oscillates around $M/(N+1)$ with the Friedel frequency $2M\pi/(N+1)$ and amplitude proportional to n^{-1} .

In summary, all our approximate formulas from the previous section are in excellent agreement with the exact results in the homogeneous case.

5.2 The Krawtchouk chain

We shall next consider the Krawtchouk chain [16, 19, 20], whose hoppings and magnetic field are given by

$$J_n = \sqrt{q(1-q)(n+1)(N-n-1)}, \quad B_n = (N-1)q + (1-2q)n \quad (56)$$

with $0 < q < 1$. This inhomogeneous chain is also exactly solvable. Indeed, the single-particle energies are the integers $0, \dots, N-1$, with corresponding eigenfunctions

$$\phi_n(\varepsilon_k) = (-1)^n \sqrt{\binom{N-1}{k} \binom{N-1}{n}} q^{\frac{1}{2}(k+n)} (1-q)^{\frac{1}{2}(N-k-n-1)} K_n(k; q, N-1).$$

Here $K_n(x; q, N-1)$ is the Krawtchouk polynomial defined by [27]

$$K_n(x; q, N-1) = {}_2F_1(-n, -x; 1-N; 1/q), \quad n = 0, \dots, N-1, \quad (57)$$

where ${}_2F_1$ is the standard hypergeometric function

$${}_2F_1(a, b; c; z) := \sum_{k=0}^{\infty} \frac{(a)_k (b)_k}{(c)_k} \frac{z^k}{k!},$$

$(a)_k := a(a+1)\cdots(a+k-1)$ being the (ascending) Pochhammer symbol. After a rescaling by $1/N$, the continuum limit of J_n and B_n are given by

$$N^{-1}J_n \rightarrow J(x) = \sqrt{q(1-q)\frac{x}{\ell}\left(1-\frac{x}{\ell}\right)}, \quad N^{-1}B_n \rightarrow B(x) = q + (1-2q)\frac{x}{\ell}.$$

Consequently, the rescaled single-particle spectrum is

$$\varepsilon_k = \frac{k}{N}, \quad k = 0, \dots, N-1, \quad (58)$$

so that the level spacing

$$\Delta\varepsilon_k = \frac{1}{N} \quad (59)$$

is constant. In particular, with this normalization

$$\nu = \frac{M}{N} = \varepsilon_M = \varepsilon_F + \frac{1}{N},$$

and thus $\nu(\varepsilon_F) = \varepsilon_F$ in the thermodynamic limit.

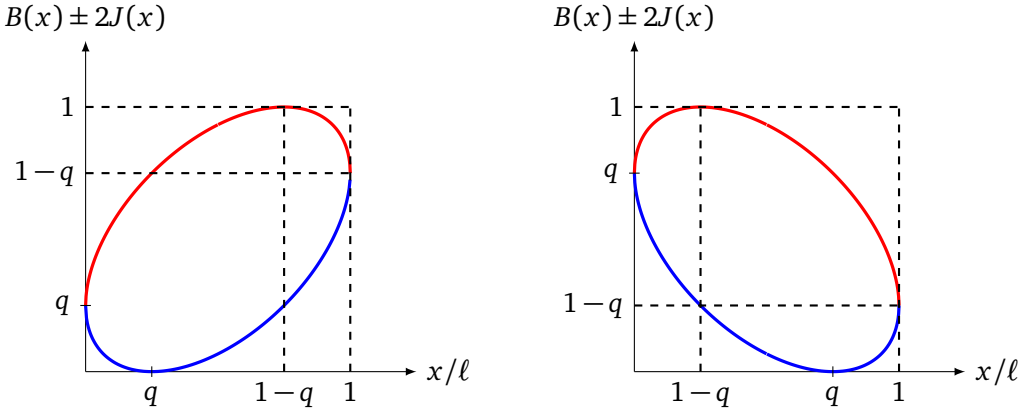


Figure 3: Plot of $B(x) + 2J(x)$ and $B(x) - 2J(x)$ (respectively in red and blue) for the Krawtchouk chain of unit length with $0 < q \leq 1/2$ (left) and $1/2 \leq q < 1$ (right).

An elementary calculation that we shall omit shows that in this case

$$\min\{B(x) - 2J(x) : x \in [0, \ell]\} = 0, \quad \max\{B(x) + 2J(x) : x \in [0, \ell]\} = 1,$$

for all $q \in [0, 1]$, as expected since the single-particle spectrum is the interval $[0, 1]$. In fact, the curve $y = B(x) \pm 2J(x)$ is an ellipse inscribed in the rectangle $[0, \ell] \times [0, 1]$ and tangent to it at the extremal points $(\ell q, 0)$ and $(\ell(1 - q), 1)$ (cf. fig. 3).

We shall next evaluate the asymptotic approximation (42) to the level spacing. To begin with, from fig. 3 it follows that in this case the region $|\xi(x, \varepsilon)| \leq 1$ consists of a single interval $[x_1(\varepsilon), x_2(\varepsilon)]$, where $x_{1,2}(\varepsilon)$ are the abscissas of the two intersection points of the horizontal line $y = \varepsilon$ with the ellipse $(y - B(x))^2 - 4J^2(x) = 0$. In other words, $x_{1,2}(\varepsilon)$ are the roots of the second-degree polynomial

$$P(x, \varepsilon) := (\varepsilon - B(x))^2 - 4J^2(x) = \frac{x^2}{\ell^2} - 2[\varepsilon(1 - 2q) + q]\frac{x}{\ell} + (\varepsilon - q)^2. \quad (60)$$

It follows that

$$(\varepsilon - B(x))^2 - 4J^2(x) = \frac{1}{\ell^2}(x - x_1(\varepsilon))(x - x_2(\varepsilon)),$$

and therefore, by eq. (35b),

$$\begin{aligned} A(\varepsilon)^{-2} &= \int_{x_1(\varepsilon)}^{x_2(\varepsilon)} \frac{dx}{\sqrt{4J(x)^2 - (\varepsilon - B(x))^2}} = \int_{x_1(\varepsilon)}^{x_2(\varepsilon)} \frac{dx}{\sqrt{-P(x, \varepsilon)}} \\ &= \ell \int_{x_1(\varepsilon)}^{x_2(\varepsilon)} \frac{dx}{\sqrt{(x - x_1(\varepsilon))(x_2(\varepsilon) - x)}}. \end{aligned}$$

The integral is easily computed with the standard change of variable

$$x = \frac{1}{2}(x_1(\varepsilon) + x_2(\varepsilon)) + \frac{1}{2}(x_2(\varepsilon) - x_1(\varepsilon)) \sin t,$$

and its value is π (independent of ε). We thus obtain

$$\Delta(\varepsilon) = \pi a A(\varepsilon)^2 = \frac{a}{\ell} = \frac{1}{N}. \quad (61)$$

Therefore in this case the asymptotic formula (42) (to lowest order in a) gives the exact value (59).

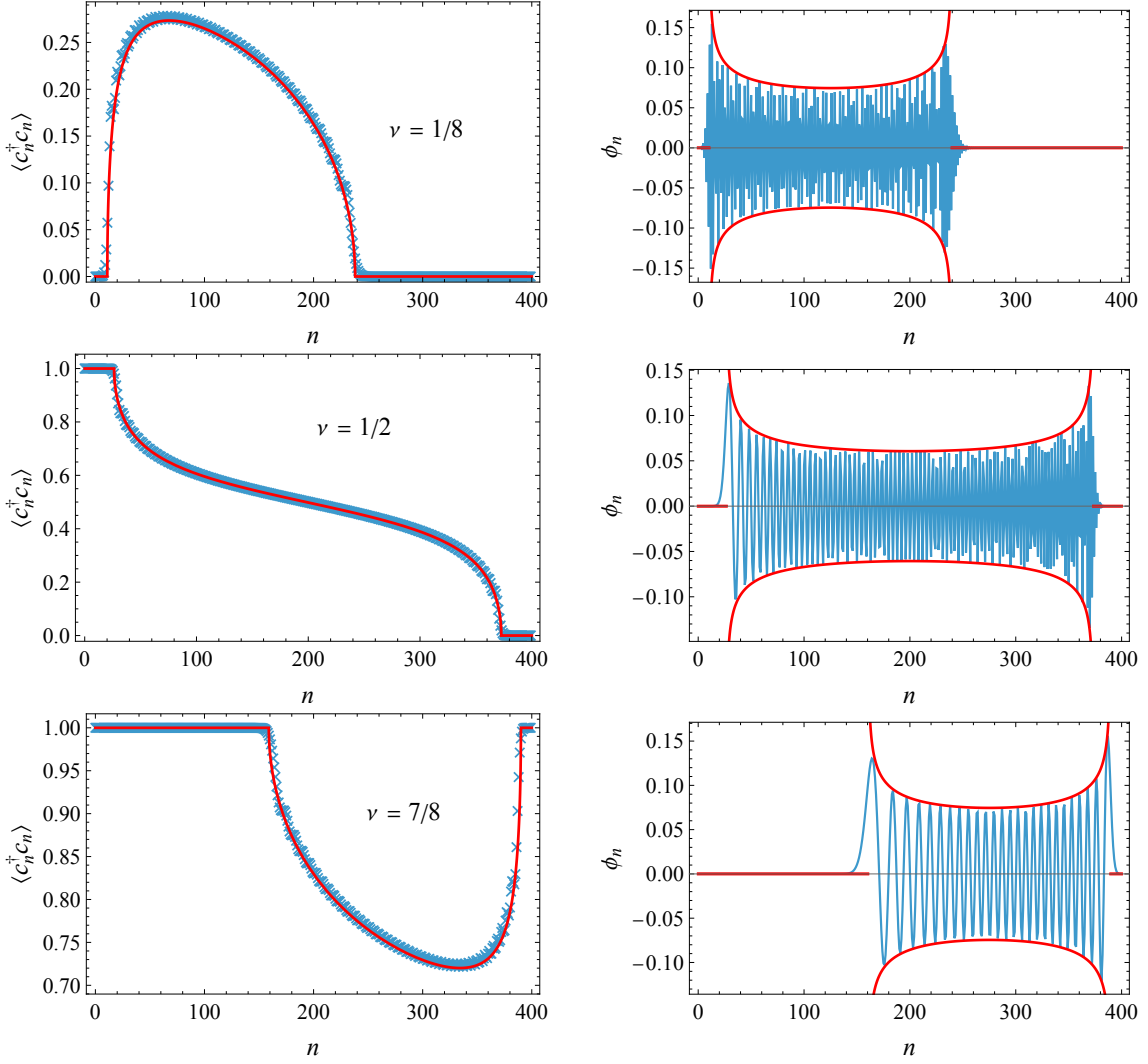


Figure 4: Left column: local fermion density for the Krawtchouk chain with $q = 1/4$, $N = 400$, and fillings $\nu = 1/8, 1/2$, and $7/8$ (blue markers), compared to its asymptotic approximation (63) (red line). Right column: analogous plot of the corresponding single-particle eigenfunctions $\phi_n(N\nu)$ (in blue) compared to their WKB envelopes (62) (red lines).

From the previous calculation it readily follows that the envelopes (36) of the WKB wave functions (35) are in this case the curves

$$y = \pm \sqrt{\frac{2}{\pi} \left[(x - x_1(\varepsilon))(x_2(\varepsilon) - x) \right]^{-1/4}}, \quad x_1(\varepsilon) < x < x_2(\varepsilon), \quad (62a)$$

where the turning points $x_{1,2}(\varepsilon)$ are explicitly given by

$$\frac{x_{1,2}(\varepsilon)}{\ell} = q + \varepsilon(1 - 2q) \pm 2\sqrt{q(1-q)\varepsilon(1-\varepsilon)}, \quad (62b)$$

cf. eq. (60) and fig. 4 (right column), where (as in the remainder of this section) we have taken $a = 1$, $\ell = N$.

Let us next analyze the behavior of the fermionic density using our asymptotic formula (50). Since the discussion is very similar for the cases $0 < q \leq 1/2$ and $1/2 \leq q < 1$, we shall restrict

in what follows to the former case. First of all, from fig. 3 it is clear that for $\varepsilon_F \in [0, 1]$ we have

$$\rho(x, \varepsilon_F) = \frac{1}{\pi a} \arccos\left(\frac{B(x) - \varepsilon_F}{2J(x)}\right), \quad x_1(\varepsilon_F) \leq x \leq x_2(\varepsilon_F), \quad (63)$$

where the turning points $x_{1,2}(\varepsilon_F)$ are given by eq. (62b). Secondly, from the definition (27) of ξ^* and fig. 3 we deduce that there are essentially three different behaviors:

- 1) $0 \leq \varepsilon_F \leq q$ (or equivalently $0 \leq \nu \leq q$, since with our normalization $\nu = \varepsilon$ in the thermodynamic limit)

In this case $\rho(x, \varepsilon_F) = 0$ for $x \in [0, x_1(\varepsilon_F)] \cup [x_2(\varepsilon_F), \ell]$, i.e., there are two depletion intervals at each end of the chain.

- 2) $q \leq \varepsilon_F \leq 1 - q$

Now $\rho(x, \varepsilon_F) = 1$ for $x \in [0, x_1(\varepsilon_F)]$ and $\rho(x, \varepsilon_F) = 0$ for $x \in [x_2(\varepsilon_F), \ell]$. In other words, there is a *saturation interval* at the left end of the chain and a depletion interval at the right end.

- 3) $1 - q \leq \varepsilon_F \leq 1$

In this case $\rho(x, \varepsilon_F) = 1$ for $x \in [0, x_1(\varepsilon_F)] \cup [x_2(\varepsilon_F), \ell]$. In other words, there are two saturation intervals at both ends of the chain.

Remark 5.1. The case $q = 1/2$ is somewhat special, since then $q = 1 - q$ and the magnetic field is constant: $B(x) = q = 1/2$. Now the range $q \leq \varepsilon_F \leq 1 - q$ reduces to the single value $\varepsilon_F = \nu = 1/2$ (half filling), for which $\xi(x, 1/2) = 0$. Hence in this case

$$a\rho(x, 1/2) = \frac{1}{2}, \quad \forall x \in [0, \ell],$$

as expected. \square

The Krawtchouk chain possesses several symmetries that we shall now briefly review. First of all, the chain parameters J_n and B_n behave under reflection about the chain's midpoint as

$$J_n \mapsto J_{N-n-2} = J_n, \quad B_n \mapsto B_{N-n-1} = N - 1 - B_n.$$

Using these relations, it is straightforward to show that⁵

$$\phi_n(k) = (-1)^n \phi_{N-n-1}(N - 1 - k). \quad (64)$$

This symmetry of the wave functions translates into a corresponding symmetry of the fermionic density. More precisely, for a Fermi energy $\varepsilon_F = M - 1$ (or filling fraction M/N), from the last equation we have

$$\begin{aligned} 1 &= \sum_{k=0}^{N-1} \phi_n^2(k) = \sum_{k=0}^{M-1} \phi_n^2(k) + \sum_{k=M}^{N-1} \phi_n^2(k) = \sum_{k=0}^{M-1} \phi_n^2(k) + \sum_{k=M}^{N-1} \phi_{N-n-1}^2(N - k - 1) \\ &= \sum_{k=0}^{M-1} \phi_n^2(k) + \sum_{k=0}^{N-M-1} \phi_{N-n-1}^2(k) = \langle M | c_n^\dagger c_n | M \rangle + \langle N - M | c_{N-n-1}^\dagger c_{N-n-1} | N - M \rangle. \end{aligned}$$

In terms of the continuum fermionic density $\rho(x, \varepsilon_F)$, the previous relation becomes

$$a\rho(x, \varepsilon_F) = 1 - a\rho(\ell - x, 1 - \varepsilon_F), \quad (65)$$

where we have taken into account that in the continuum limit the energies are rescaled by a factor N^{-1} (cf. (58)). To check that this symmetry is shared by the WKB approximation to the fermionic density, note first of all that $J(x) = J(\ell - x)$ and $B(\ell - x) = 1 - B(x)$, and therefore

$$\xi(\ell - x, 1 - \varepsilon_F) = -\xi(x, \varepsilon_F).$$

⁵Recall that in this case (with the normalization (56)) the chain energies are the numbers $\varepsilon_k = k$, with $k = 0, \dots, N - 1$

Since $x_{1,2}(1 - \varepsilon_F) = \ell - x_{2,1}(\varepsilon_F)$, from eq. (63) we obtain

$$a\rho(\ell - x, 1 - \varepsilon_F) = \frac{1}{\pi} \arccos \xi(x, \varepsilon_F) = \frac{1}{\pi} (\pi - \arccos(-\xi(x, \varepsilon_F))) = 1 - a\rho(x, \varepsilon_F),$$

as claimed. In fact, the symmetry (65) is apparent from the plots presented in fig. 4 (left column).

Likewise, under the parameter reflection $q \mapsto 1 - q$ we have

$$J_n \mapsto J_n, \quad B_n \mapsto N - 1 - B_n,$$

From these equations it is straightforward to derive the following relation between the single-particle wave functions with parameters q and $1 - q$:

$$\phi_n(k; 1 - q) = (-1)^n \phi_n(N - 1 - k; q),$$

which combined with eq. (64) yields the identity

$$\phi_n(k; 1 - q) = \phi_{N-n-1}(k; q).$$

In the continuum limit (after rescaling of the energies by N^{-1}), this relation yields

$$\rho(x, \varepsilon_F; 1 - q) = \rho(\ell - x, \varepsilon_F; q). \quad (66)$$

To show that the last equation is satisfied by the WKB approximation to the fermionic density, it suffices to note that

$$J(x; 1 - q) = J(\ell - x; q), \quad B(x; 1 - q) = B(\ell - x, q),$$

and therefore $\xi(x, \varepsilon; 1 - q) = \xi(\ell - x, \varepsilon; q)$. Equation (66) then follows immediately from eq. (63), taking into account that $x_{1,2}(\varepsilon_F; 1 - q) = \ell - x_{2,1}(\varepsilon_F; q)$.

5.3 The rainbow chain

The rainbow chain was introduced in 2010 by Vitagliano and collaborators [6] to illustrate violations of the area law, and has since been extensively studied [7, 8, 18, 28–30]. We shall take the model's parameters as

$$J_n = \frac{1}{2} \exp \left(-h \left| \frac{1}{2} - \frac{n}{N} + \frac{1}{2N} \delta_{n, N/2-1} \right| \right), \quad B_n = 0,$$

where $h > 0$ and N is even. The continuum limit of these parameters is therefore

$$J(x) = \frac{1}{2} e^{-h|\frac{1}{2} - \frac{x}{\ell}|}, \quad B(x) = 0,$$

so that, by eq. (32), in the thermodynamic limit the single-particle energies should lie in the interval $[-1, 1]$.

We shall start by evaluating the approximation to the single-particle level density $D(\varepsilon)$ in eq. (42). By the particle-hole symmetry discussed in remark 4.4, we can restrict ourselves without loss of generality to negative energies. From the graph of $\pm 2J(x)$ (see fig. 5) it is then apparent that there are essentially two regimes:

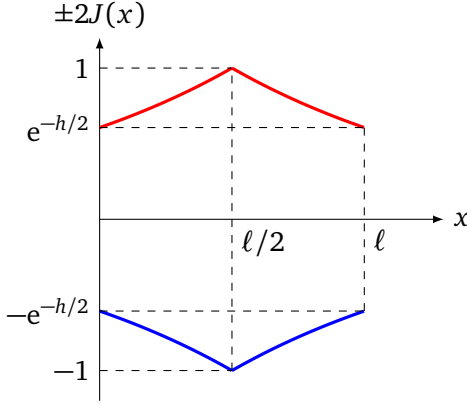


Figure 5: Schematic plot of $\pm 2J(x)$ for the rainbow chain.

1) $-1 \leq \varepsilon \leq -e^{-h/2}$

In this case $\xi(x, \varepsilon) < -1$ for $x \in (0, x_1(\varepsilon)) \cup (x_2(\varepsilon), \ell)$, where the turning points $x_{1,2}(\varepsilon)$ are given by

$$x_{1,2}(\varepsilon) = \frac{\ell}{2} \pm \frac{\ell}{h} \log |\varepsilon|. \quad (67)$$

From eq. (35b) and the symmetry of $J(x)$ under reflections about $x = \ell/2$ it then follows that

$$A(\varepsilon)^{-2} = 2 \int_{x_1(\varepsilon)}^{\ell/2} \frac{dx}{\sqrt{4J^2(x) - \varepsilon^2}} = 2\ell \int_{x_1(\varepsilon)/\ell}^{1/2} \frac{dx}{\sqrt{e^{-h(1-2x)} - \varepsilon^2}} = \frac{\ell}{h} \int_0^{-2\log|\varepsilon|} \frac{ds}{\sqrt{e^{-s} - \varepsilon^2}}.$$

Evaluating the integral we thus obtain

$$D(\varepsilon) = \frac{1}{\pi a} A(\varepsilon)^{-2} = \frac{\ell}{ha|\varepsilon|} \left(1 - \frac{2}{\pi} \arcsin |\varepsilon| \right), \quad -1 \leq \varepsilon \leq -e^{-h/2}. \quad (68)$$

2) $-e^{-h/2} \leq \varepsilon \leq 0$

Now $|\xi(x, \varepsilon)| \leq 1$ for all $x \in [0, \ell]$, and therefore

$$A(\varepsilon)^{-2} = 2 \int_0^{\ell/2} \frac{dx}{\sqrt{4J^2(x) - \varepsilon^2}} = \frac{\ell}{h} \int_0^h \frac{ds}{\sqrt{e^{-s} - \varepsilon^2}},$$

and hence

$$D(\varepsilon) = \frac{1}{\pi a} A(\varepsilon)^{-2} = \frac{2\ell}{\pi ha|\varepsilon|} \left(\arcsin(e^{h/2}|\varepsilon|) - \arcsin|\varepsilon| \right), \quad -e^{-h/2} \leq \varepsilon \leq 0. \quad (69)$$

Combining the value of $A(\varepsilon)$ just computed with eq. (36) we obtain the following explicit equation for the envelopes of the single-particle approximate eigenfunctions:

$$y = \pm \sqrt{\frac{h|\varepsilon|}{\ell}} \left(e^{-h|1-\frac{2x}{\ell}|} - \varepsilon^2 \right)^{-1/4} \begin{cases} \left(\frac{\pi}{2} - \arcsin|\varepsilon| \right)^{-1/2}, & e^{-h/2} \leq |\varepsilon| \leq 1 \\ \left(\arcsin(e^{h/2}|\varepsilon|) - \arcsin|\varepsilon| \right)^{-1/2}, & |\varepsilon| \leq e^{-h/2}, \end{cases} \quad (70)$$

where in the first line it is understood that $y = 0$ for $x \notin [x_1(\varepsilon), x_2(\varepsilon)]$. As an example, in fig. 6 we show these envelopes together with the graphs of the corresponding numerical single-particle eigenfunctions for a chain of $N = 400$ spins with parameter $h = 1$, at the energies $\varepsilon_{N/8}$ and $\varepsilon_{2N/5}$. In particular, it is apparent from these plots that $y(x) = y(\ell - x)$, which is a direct

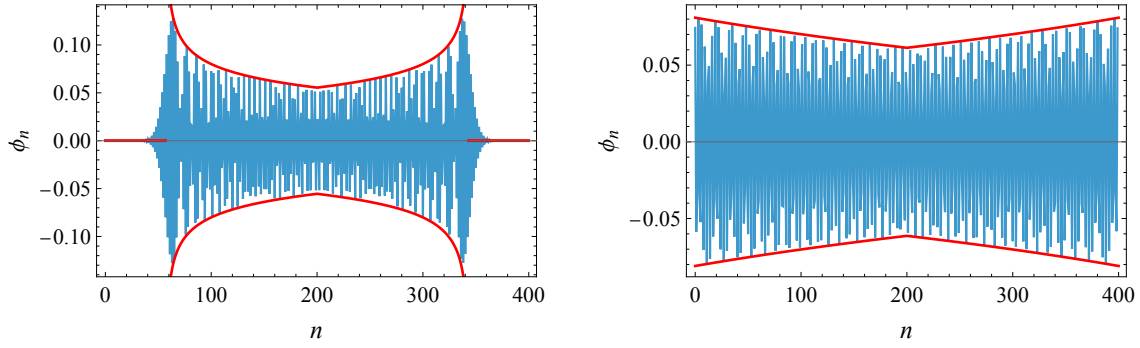


Figure 6: Single-particle eigenfunctions $\phi_n(\varepsilon)$ with energies $\varepsilon = N/8$ (left) and $\varepsilon = 2N/5$ (right) for the rainbow chain with $h = 1$, $N = 400$, compared to the envelopes (70) of the corresponding approximate WKB wave functions (red lines).

consequence of the symmetry of the coupling $J(x)$ about the chain's midpoint. (This is also obvious from eq. (70).)

We shall next evaluate the approximation (47) to the filling fraction $\nu(\varepsilon_F)$ at a Fermi energy ε_F , supposing again without loss of generality that $\varepsilon_F \leq 0$. If $-1 \leq \varepsilon_F \leq -e^{-h/2}$ then $\xi^*(x, \varepsilon_F) = -1$ outside the interval $(x_1(\varepsilon_F), x_2(\varepsilon_F))$, and therefore (again by symmetry about $x = \ell/2$)

$$\begin{aligned} \nu(\varepsilon_F) &= \frac{2}{\pi\ell} \int_{x_1(\varepsilon_F)}^{\ell/2} dx \arccos(-\xi(x, \varepsilon_F)) = \frac{2}{\pi} \int_{x_1(\varepsilon_F)/\ell}^{1/2} dx \arccos\left(e^{h(\frac{1}{2}-x)} |\varepsilon_F|\right) \\ &= \frac{2}{\pi h} \int_{|\varepsilon_F|}^1 \frac{ds}{s} \arccos s = \frac{2}{\pi h} \int_{|\varepsilon_F|}^1 \frac{ds}{s} \left(\frac{\pi}{2} - \arcsin s\right) = -\frac{1}{h} \log |\varepsilon_F| - \frac{2}{\pi h} f(|\varepsilon_F|), \end{aligned}$$

where

$$f(t) := \int_t^1 \frac{ds}{s} \arcsin s.$$

In fact, the RHS can be evaluated in closed form in terms of Clausen's integral

$$\text{Cl}_2(\theta) := - \int_0^\theta dx \log\left(2 \sin \frac{x}{2}\right) = \sum_{n=1}^{\infty} \frac{\sin(n\theta)}{n^2}, \quad 0 < \theta < 2\pi,$$

which is in turn related to the standard dilogarithm function [23] by

$$\text{Cl}_2(\theta) = \text{Im} \text{Li}_2(e^{i\theta}) = \frac{1}{2i} (\text{Li}_2(e^{i\theta}) - \text{Li}_2(e^{-i\theta})).$$

More precisely,

$$f(t) = \frac{\pi}{2} \log 2 - \log(2t) \arcsin t - \frac{1}{2} \text{Cl}_2(2 \arcsin t),$$

and hence

$$\begin{aligned} \nu(\varepsilon_F) &= -\frac{1}{h} \log |2\varepsilon_F| \\ &\quad + \frac{1}{\pi h} \left(2 \log |2\varepsilon_F| \arcsin |\varepsilon_F| + \text{Cl}_2(2 \arcsin |\varepsilon_F|) \right), \quad -1 \leq \varepsilon_F \leq -e^{-h/2}. \end{aligned} \quad (71)$$

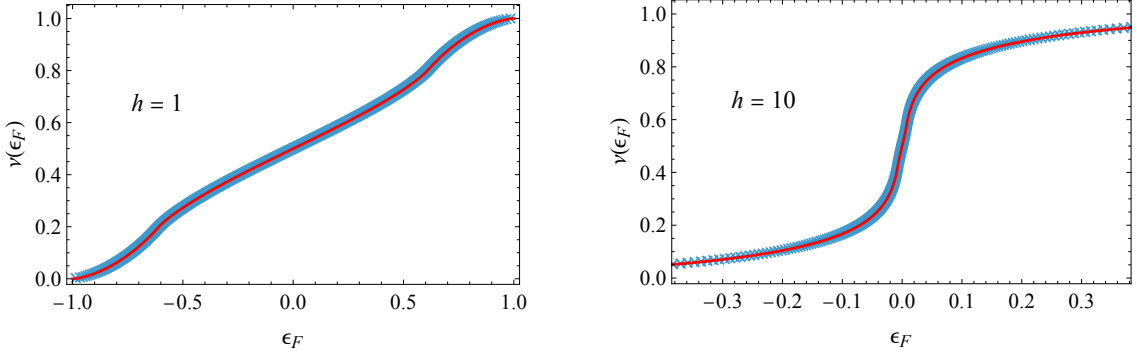


Figure 7: Filling fraction ν vs. Fermi energy ϵ_F for the rainbow chain with $N = 400$ spins and parameters $h = 1, 10$ (blue markers), compared to their WKB approximation (71)-(72) (red line).

Consider next the case $-e^{-h/2} \leq \epsilon_F \leq 0$, in which $|\xi(x, \epsilon_F)| \leq 1$ for all $x \in [0, \ell]$. Now

$$\begin{aligned} \nu(\epsilon_F) &= \frac{2}{\pi\ell} \int_0^{\ell/2} dx \arccos(-\xi(x, \epsilon_F)) = \frac{2}{\pi} \int_0^{1/2} dx \arccos(e^{h(\frac{1}{2}-x)} |\epsilon_F|) \\ &= \frac{2}{\pi h} \int_{|\epsilon_F|}^{e^{h/2}|\epsilon_F|} \frac{ds}{s} \arccos s = \frac{2}{\pi h} \int_{|\epsilon_F|}^{e^{h/2}|\epsilon_F|} \frac{ds}{s} \left(\frac{\pi}{2} - \arcsin s \right) \\ &= \frac{1}{2} + \frac{2}{\pi h} \left(f(e^{h/2} |\epsilon_F|) - f(|\epsilon_F|) \right). \end{aligned} \quad (72)$$

In fact, our numerical calculations show that the approximation (71)-(72) (extended to positive energies using eq. (53)) is remarkably accurate across the full energy range $\epsilon_F \in [-1, 1]$; see, e.g., fig. 7 for the cases $h = 1$ and $h = 10$.

We shall finally discuss the approximation to the fermionic density given by eq. (50). From fig. 5 it is clear that in the range $-1 \leq \epsilon_F \leq -e^{-h/2}$ we have $\arccos(-\xi^*(\epsilon_F)) = 0$ for $x \notin (x_1(\epsilon_F), x_2(\epsilon_F))$. Hence in this case there are two depletion intervals at the two ends of the chain, limited by the turning points $x_{1,2}(\epsilon_F)$, while in the interval $[x_1(\epsilon_F), x_2(\epsilon_F)]$ we have

$$a\rho(x, \epsilon_F) = \frac{1}{\pi} \arccos(|\epsilon_F| e^{h|\frac{1}{2}-\frac{x}{\ell}|}). \quad (73)$$

Note that $\rho(x, \epsilon_F)$ is clearly symmetric about $x = \ell/2$, as expected by the analogous symmetry of $J(x)$. On the other hand, for $-e^{-h/2} \leq \epsilon_F \leq 0$ there are no depletion intervals, since $|\xi(x, \epsilon_F)| \leq 1$ for all $x \in [0, \ell]$, so that the last equation is valid in the whole interval $[0, \ell]$. Of course, the fermionic density for positive energies can be computed from the symmetry relation (53).

In fig. 8 we have plotted the fermionic density of the rainbow chain with $N = 400$ spins and parameter $h = 1$ for the fillings $\nu = 1/8$ and $\nu = 2/5$, compared to its approximation (73). For these values of N and h we have $e^{-h/2} = 0.60653\dots$, so that the corresponding Fermi energies satisfy $\epsilon_F(1/8) = -0.69945 < -e^{-h/2}$ and $\epsilon_F(2/5) = -0.24004 > -e^{-h/2}$, respectively. Thus for $\nu = 1/8$ there are two depletion intervals, namely (by eq. (67)) $[0, 57.018]$ and $[342.982, 400]$, while for $\nu = 2/5$ there are none. As can be seen from fig. 8, this prediction is borne out by the numerical data. In fact, the approximation (73) is reasonably accurate for both values of ν , although for $\nu = 2/5$ characteristic Friedel oscillations appear at the chain's ends.

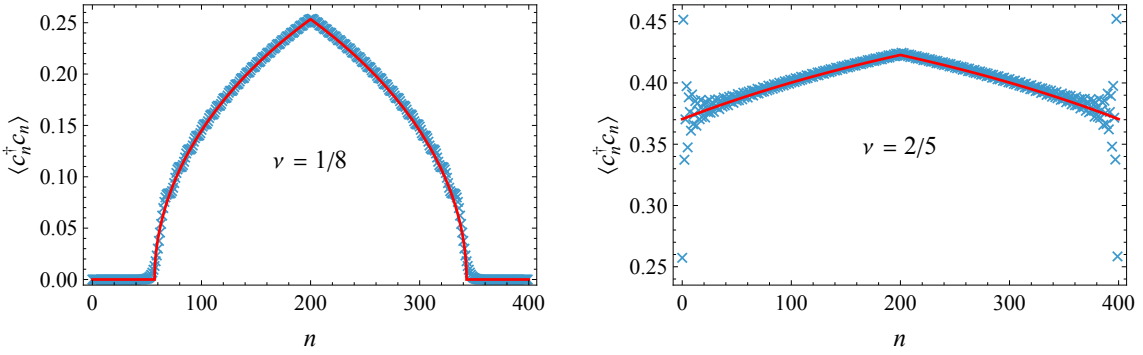


Figure 8: Local fermion density for the rainbow chain with $h = 1$, $N = 400$, and filling fractions $\nu = 1/8$ and $2/5$ (blue markers) compared to its asymptotic approximation (73) (red line).

5.4 The cosine chain

Consider next the cosine chain introduced in ref. [17], with parameters

$$J_n = 1 + J_0 \cos\left(\frac{2\pi n}{N}\right), \quad B_n = 0, \quad (74)$$

whose continuum limit is given by

$$J(x) = 1 + J_0 \cos\left(\frac{2\pi x}{\ell}\right), \quad B(x) = 0. \quad (75)$$

Note that this chain's hoppings are *not* symmetric about its midpoint (i.e., J_n is not invariant under the reflection $n \mapsto N - 2 - n$), although their continuum counterparts (75) are. By eq. (32), the single-particle spectrum lies inside the interval $[-2 - 2J_0, 2 + 2J_0]$. It is apparent from fig. 9 that the qualitative behavior of the fermionic density depends on whether the Fermi energy ε_F is smaller or larger in absolute value than $2 - 2J_0$. Indeed, in the former case, i.e., for $-2 + 2J_0 \leq \varepsilon_F \leq 2 - 2J_0$, there are no depletion/saturation regions, and the fermionic density is given by

$$\rho(x, \varepsilon_F) = \frac{1}{\pi a} \arccos\left(\frac{|\varepsilon_F|/2}{1 + J_0 \cos\left(\frac{2\pi x}{\ell}\right)}\right) \quad (76)$$

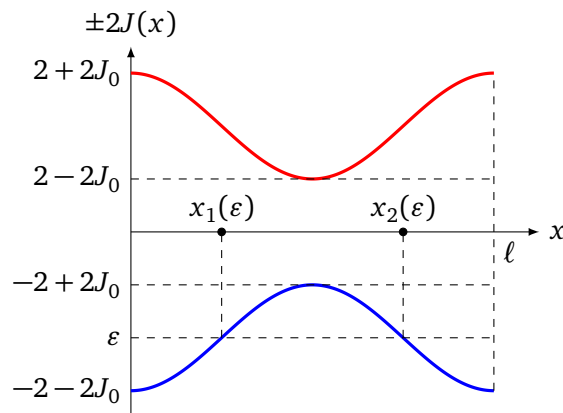


Figure 9: Plot of $\pm 2J(x)$ for the cosine chain (75), showing the turning points $x_{1,2}(\varepsilon)$ for the specified energy ε .

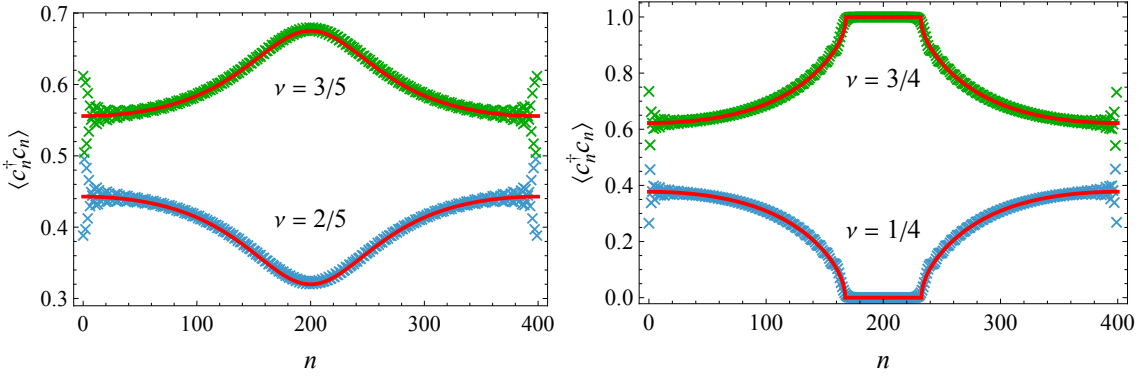


Figure 10: Local fermion density for the cosine chain (74) with $J_0 = 1/2$, $N = 400$ spins, and several values of the filling ν (blue and green markers) compared to their WKB approximation (50) (continuous red line).

for all $x \in [0, \ell]$. For instance, for $\varepsilon_F \in [-2 + 2J_0, 0]$, ρ decreases monotonically over the interval $[0, \ell/2]$ from its maximum value $\rho(0, \varepsilon_F) = (\pi a)^{-1} \arccos\left(\frac{|\varepsilon_F|}{2(1+J_0)}\right)$ to its minimum $\rho(\ell/2, \varepsilon_F) = (\pi a)^{-1} \arccos\left(\frac{|\varepsilon_F|}{2(1-J_0)}\right)$, and is symmetric about $\ell/2$ (see, e.g., fig. 10, left panel, with $\nu = 2/5$, for which $\varepsilon_F = -0.53597 \in [-2 + 2J_0, 0] = [-1, 0]$). The behavior of ρ for $\varepsilon_F \in [0, 2 - 2J_0]$ is completely analogous (see fig. 10, left panel, with $\nu = 3/5$, for which $\varepsilon_F = 0.52343 \in [0, 2 - 2J_0] = [0, 1]$). A special case occurs when $\varepsilon_F = 0$ (i.e., at half filling), when $\rho(x, 0) = 1/(2a)$ becomes constant. On the other hand, for ε_F in the range $[-2 - 2J_0, -2 + 2J_0]$ or $[2 - 2J_0, 2 + 2J_0]$ there are two turning points $x_{1,2}(\varepsilon_F)$ given by

$$x_1(\varepsilon_F) = \frac{\ell}{2\pi} \arccos\left(\frac{|\varepsilon_F| - 2}{2J_0}\right), \quad x_2(\varepsilon_F) = \ell - x_1(\varepsilon_F) \quad (77)$$

(cf. fig. 9). In this case $[x_1(\varepsilon_F), x_2(\varepsilon_F)]$ is a depletion interval for $\varepsilon_F \in [-2 - 2J_0, -2 + 2J_0]$ and a saturation interval for $\varepsilon_F \in [2 - 2J_0, 2 + 2J_0]$. Outside this interval, the fermionic density is again given by eq. (76); see, e.g., fig. 10, right panel, with filling fractions corresponding to the energies -1.12833 and 1.12323 .

We have been able to obtain closed-form expressions for the normalization constant $A(\varepsilon)$ —and, hence, for the equation (36) of the WKB envelopes—in terms of a complete elliptic integral of the first kind, but we shall omit them here due to their excessive complexity. More

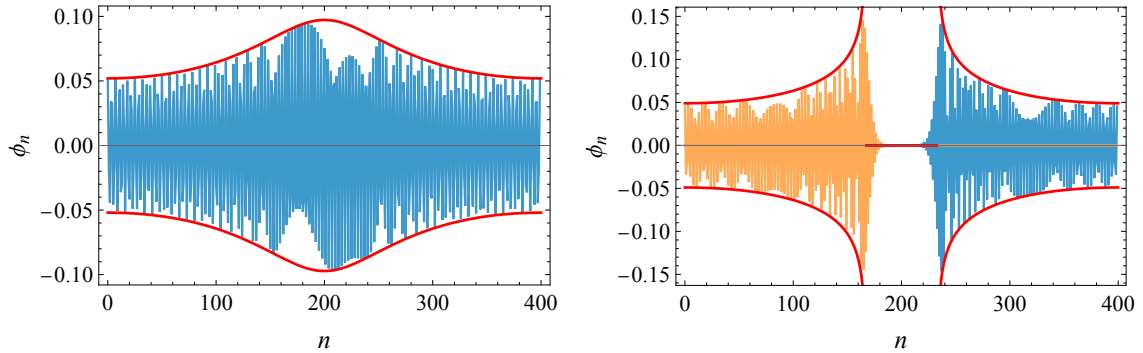


Figure 11: WKB envelopes (36) for the cosine chain (74) with $J_0 = 1/2$ and $N = 400$ spins (red lines), compared to the exact wave function $\phi_n(\varepsilon_{2N/5})$ (left) and the linear combination with equal coefficients $1/\sqrt{2}$ of the exact eigenfunctions $\phi_n(\varepsilon_{N/4})$ (right panel, blue) and $\phi_n(\varepsilon_{N/4+1})$ (right panel, orange).

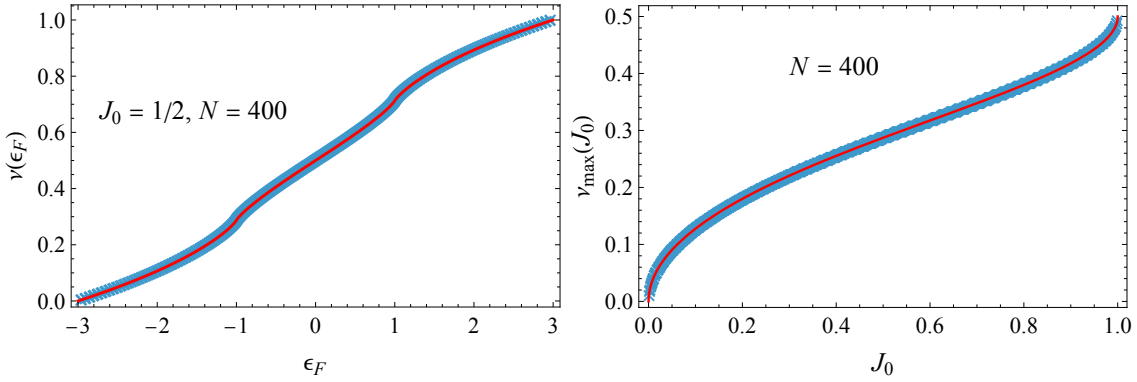


Figure 12: Left: filling fraction $\nu(\epsilon_F)$ for the cosine chain (74) with $J_0 = 1/2$ and $N = 400$ spins (blue markers) compared to its WKB approximation (47). Right: maximum filling fraction $\nu_{\max}(J_0)$ for which the fermionic density exhibits depletion for $N = 400$ and $J_0 = 0.001, 0.002, \dots, 0.999$ (blue markers), compared to its WKB approximation (78) (red line).

precisely, from the discussion in section 3 and remark 4.2, it follows that when there is no depletion/saturation, i.e., for $|\epsilon| < 2 - 2J_0$, these curves are genuine envelopes for the corresponding eigenfunctions, while for $|\epsilon| \geq 2 - 2J_0$ they are the envelopes of the linear combinations $(\phi_n(\epsilon_k) + \phi_n(\epsilon_{k+1}))/\sqrt{2}$ of two neighboring eigenfunctions (cf. fig. 11).

Although we have not found an explicit expression for the filling fraction $\nu(\epsilon_F)$ in terms of the Fermi energy ϵ_F , it can of course be evaluated numerically without difficulty for given ϵ_F and J_0 from eq. (47) (see, e.g., fig. 12 (left) for a plot of the filling fraction $\nu(\epsilon_F)$ for $J_0 = 1/2$ and $N = 400$ spins compared to its WKB approximation). In particular, the maximum filling fraction $\nu_{\max}(J_0)$ for which the fermionic density features a depletion interval, given by the integral

$$\nu_{\max}(J_0) = \frac{1}{\pi\ell} \int_0^\ell dx \arccos(-\xi(2J_0 - 2)) = \frac{1}{\pi^2} \int_0^\pi ds \arccos\left(\frac{1 - J_0}{1 + J_0 \cos s}\right), \quad (78)$$

can be computed in this way for any $J_0 \in (0, 1)$ (see fig. 12 (right) for the graph of this function for $N = 400$ spins).

5.5 An asymmetric cosine chain

As our last example, we shall consider the generalization of the cosine chain discussed above with parameters

$$J_n = 1 + J_0 \cos\left(\frac{2\pi rn}{N}\right), \quad B_n = b\left(\frac{n}{N}\right)^2, \quad (79a)$$

where for definiteness we have taken

$$J_0 = \frac{3}{4}, \quad b = 5, \quad r = 2. \quad (79b)$$

The continuum version of the chain parameters is therefore given by

$$J(x) = 1 + J_0 \cos\left(\frac{2\pi rx}{\ell}\right), \quad B(x) = b\left(\frac{x}{\ell}\right)^2. \quad (80)$$

Hence in this example neither the chain's parameters (79) nor their continuum counterparts (80) are symmetric about the chain's midpoint. In fig. 13 we have plotted the graphs of

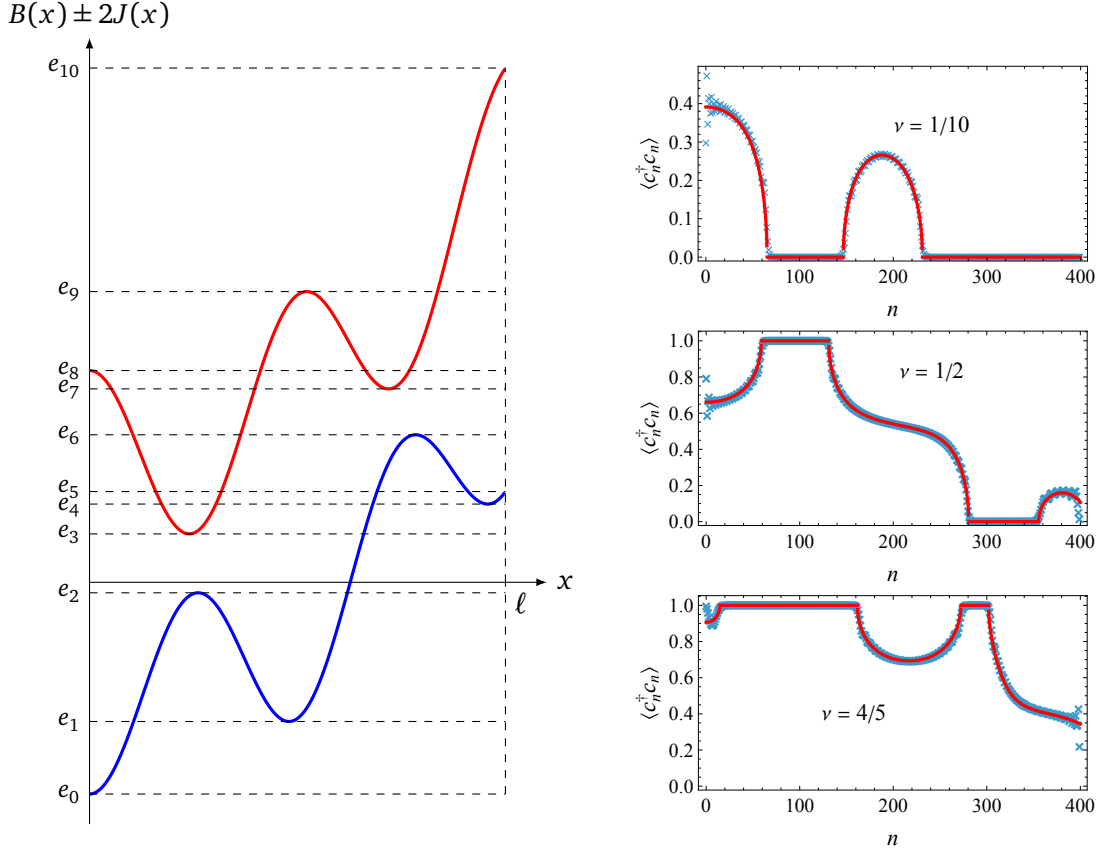


Figure 13: Left: plot of $B(x) \pm 2J(x)$ for the general cosine chain (79). The qualitative behavior of the fermionic density is determined by the interval $[e_i, e_{i+1}]$ (with $i = 0, 1, \dots, 9$) containing the Fermi energy ε_F . Right: local fermion density for the chain (79) with $N = 400$ spins for several filling fractions (blue markers), compared to its WKB approximation (50) (red line).

the functions $B(x) \pm 2J(x)$ which, as discussed above, determine the different qualitative behaviors of the fermionic density. More specifically, the behavior of $\rho(x, \varepsilon_F)$ depends on the interval $[e_i, e_{i+1}]$ containing the Fermi energy ε_F , where e_j (with $j = 0, 1, \dots, 10$) is one of the energies plotted in fig. 13 (the numerical values of these energies and their corresponding filling fractions are listed in table 1). For instance, if $e_5 < \varepsilon_F < e_6$ (i.e., for filling fractions between $\nu_5 = 0.4725$ and $\nu_6 = 0.6225$) there are four turning points $x_i(\varepsilon_F)$ ($i = 1, \dots, 4$), with $x_1(\varepsilon_F) > 0$ and $x_4(\varepsilon_F) < \ell$. The fermionic density features a saturation interval $[x_1(\varepsilon_F), x_2(\varepsilon_F)]$ and a depletion interval $[x_3(\varepsilon_F), x_4(\varepsilon_F)]$, while it varies continuously over the intervals $[0, x_1(\varepsilon_F)]$, $[x_2(\varepsilon_F), x_3(\varepsilon_F)]$, and $[x_4(\varepsilon_F), \ell]$.

As in the previous examples, the WKB approximations derived in the previous section are in excellent agreement with the numerical results. For instance, in fig. 14 (left) we compare the WKB envelopes (36) with $\varepsilon = \varepsilon_{N/2}$ (for a chain with $N = 400$ spins) with the linear com-

Table 1: Critical values e_i of the Fermi energy (with $i = 1, \dots, 9$) and their corresponding filling fraction ν_i .

e_i	-2.3009	-0.1737	0.7998	1.2929	1.5000	2.4384	3.1972	3.5000	4.8055
ν_i	0.0225	0.2100	0.3700	0.4425	0.4725	0.6225	0.7700	0.8225	0.9350

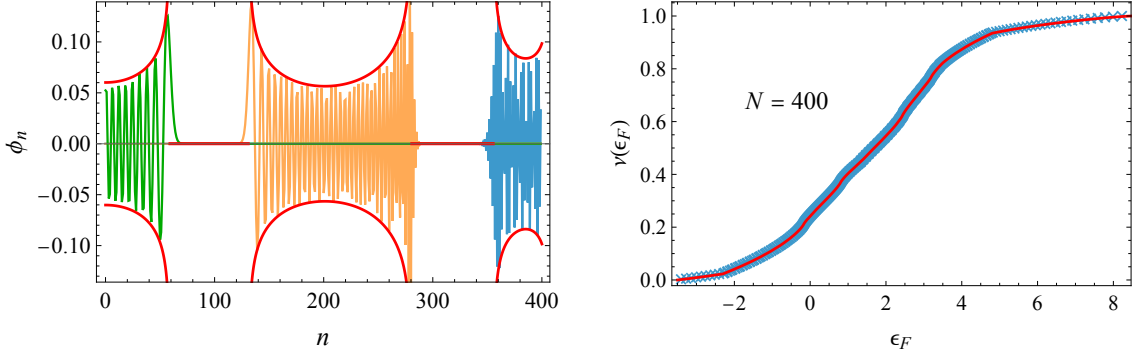


Figure 14: Left: linear combination (81) of the exact eigenfunctions of the chain (79) with $N = 400$ and energies $\varepsilon_{N/2}$ (blue), $\varepsilon_{N/2+1}$ (orange) and $\varepsilon_{N/2+2}$ (green), compared to its WKB envelope (36) (red curve). Right: filling fraction $\nu(\varepsilon_F)$ as a function of the Fermi energy ε_F (blue markers) compared to its WKB approximation (47) (red line).

bination of three exact eigenfunctions with consecutive energies $\varepsilon_{N/2+i}$ ($i = 0, 1, 2$), weighted as explained in remark 4.2. More precisely, from fig. 13 and table 1 it follows that for the energy $\varepsilon_{N/2} = 1.69251 \in (e_5, e_6)$ there are four turning points x_1, \dots, x_4 and three potential wells $I_1 = [0, x_1]$, $I_2 = [x_2, x_3]$ and $I_3 = [x_4, \ell]$. As illustrated in fig. 14 (left), the three exact eigenfunctions $\phi_n(\varepsilon_{N/2})$, $\phi_n(\varepsilon_{N/2+1})$, and $\phi_n(\varepsilon_{N/2+2})$ are respectively localized in the wells I_3 , I_2 , and I_1 . According to remark 4.2 (see, in particular, eq. (48)), eq. (36) with $\varepsilon = \varepsilon_{N/2}$ should provide a good approximation to the envelope of the linear combination⁶

$$\sum_{i=1}^3 \frac{A(\varepsilon_{N/2})}{A_i(\varepsilon_{N/2})} \phi_n(\varepsilon_{N/2+i}) \quad (81)$$

(cf. eq. (48)). This is in fact borne out by the figure.

It is also straightforward to obtain an estimate of the fermionic density for a given filling fraction ν (or Fermi energy ε_F) using eq. (50). This formula is surprisingly accurate over the whole range of filling fractions, as can be seen from fig. 13 (right). Finally, by numerically integrating eq. (47) it is possible to derive an excellent asymptotic approximation to the filling fraction $\nu(\varepsilon_F)$ for arbitrary Fermi energy (see, e.g., fig. 14 (right) for $N = 400$ spins).

6 Conclusions and outlook

In this work, we developed a new analytical approach to study the fermion density profile of inhomogeneous XX spin chains in the thermodynamic limit. By applying a WKB-like approximation directly to the three-term recurrence relations satisfied by the single-particle eigenfunctions, we constructed continuous approximations to these eigenfunctions without resorting to the associated field theory. This led to a simple and general closed-form expression for the local fermion density as a function of the Fermi energy, valid for arbitrary fillings, site-dependent hopping amplitudes, and external magnetic fields.

Our density formula accurately captures both the depletion and saturation phenomena that were previously observed numerically, but were not well understood analytically away from criticality beyond the low-filling, zero-field regime. By testing the formula on a wide range of inhomogeneous chains, including the Krawtchouk, rainbow, cosine, and (in the Supplementary

⁶Recall that we are taking $a = 1$, and therefore $\ell = N$.

Material) Rindler chains, we demonstrated the excellent agreement of our asymptotic formula with the numerical results even for moderately large systems.

In addition to its practical utility, our method may shed light on the mechanisms behind entanglement suppression in inhomogeneous XX spin chains. For instance, in the simplest case in which the eigenfunctions are localized in a single interval, the correlation matrix C_{nm} can be approximated in the thermodynamic limit as follows:

$$C_{nm} \equiv \langle M | c_n^\dagger c_m | M \rangle \rightarrow C(x, y) = a \int_{\varepsilon_0}^{\varepsilon_F} d\varepsilon D(\varepsilon) \phi(x, \varepsilon) \phi(y, \varepsilon) = \frac{1}{\pi} \int_{\varepsilon_0}^{\varepsilon_F} d\varepsilon f(x, \varepsilon) f(y, \varepsilon), \quad (82a)$$

where $x = na$, $y = ma$, $\varepsilon_F = \varepsilon_{M-1}$, and

$$f(s, \varepsilon) = \frac{\sin \varphi^*(s, \varepsilon)}{\sqrt{J(s)(1 - \xi(s, \varepsilon)^2)^{1/2}}} \Theta(1 - \xi(s, \varepsilon)^2). \quad (82b)$$

Since the eigenstates of free-fermion systems are Gaussian [14], the two-point correlation matrix determines all higher-order correlations and entanglement properties. In particular, as explained in section 2, the entanglement entropy of a subset $A \subset \{0, \dots, N-1\}$ can be efficiently evaluated through eq. (13) in terms of the eigenvalues ν_j of the truncated correlation matrix $\mathbf{C}_A = (C_{nm})_{n,m \in A}$. In this way eqs. (82) could be the starting point for deriving asymptotic approximations to the bipartite entanglement entropy for arbitrary fillings and external magnetic fields, where the standard field-theoretic techniques based on conformal field theory [31, 32] are not directly applicable due to the lack of conformal invariance. This could be of particular interest in the study of the asymptotic growth of the entanglement entropy with the block size away from criticality, which in simple cases has been observed to follow the usual area law for one-dimensional critical systems [7, 8, 31–33] rescaled to the non-depletion region [16].

Funding information This work was partially supported by grants PID2024-155527NB-I00 from Spain’s Ministerio de Ciencia, Innovación y Universidades and PR12/24-31565 from Universidad Complutense de Madrid.

Supplementary Material

An additional worked example presenting the computation of the fermionic density of the Rindler chain for several values of its parameter is available at [Zenodo repository](#).

References

- [1] T. Graß and M. Lewenstein, *Trapped-ion quantum simulation of tunable-range Heisenberg chains*, EPJ Quantum Technology **1**, 8(20) (2014), doi:[10.1140/epjqt8](https://doi.org/10.1140/epjqt8).
- [2] R. E. Barfknecht, T. Mendes-Santos and L. Fallani, *Engineering entanglement Hamiltonians with strongly interacting cold atoms in optical traps*, Phys. Rev. Res. **3**, 013112 (2021), doi:[10.1103/PhysRevResearch.3.013112](https://doi.org/10.1103/PhysRevResearch.3.013112).
- [3] J. Rodríguez-Laguna, L. Tarruell, M. Lewenstein and A. Celi, *Synthetic Unruh effect in cold atoms*, Phys. Rev. A **95**, 013627 (2017), doi:[10.1103/PhysRevA.95.013627](https://doi.org/10.1103/PhysRevA.95.013627).

[4] F. Schäfer, T. Fukuhara, S. Sugawa, Y. Takasu and Y. Takahashi, *Tools for quantum simulation with ultracold atoms in optical lattices*, Nat. Rev. Phys. **2**, 411 (2020), doi:[10.1038/s42254-020-0195-3](https://doi.org/10.1038/s42254-020-0195-3).

[5] C. Monroe, W. C. Campbell, L.-M. Duan, Z.-X. Gong, A. V. Gorshkov, P. W. Hess, R. Islam, K. Kim, N. M. Linke, G. Pagano, P. Richerme, C. Senko *et al.*, *Programmable quantum simulations of spin systems with trapped ions*, Rev. Mod. Phys. **93**, 025001 (2021), doi:[10.1103/RevModPhys.93.025001](https://doi.org/10.1103/RevModPhys.93.025001).

[6] G. Vitagliano, A. Riera and J. I. Latorre, *Volume-law scaling for the entanglement entropy in spin-1/2 chains*, New J. Phys. **12**, 113049(16) (2010), doi:[10.1088/1367-2630/12/11/113049](https://doi.org/10.1088/1367-2630/12/11/113049).

[7] J. Rodríguez-Laguna, J. Dubail, G. Ramírez, P. Calabrese and G. Sierra, *More on the rainbow chain: entanglement, space-time geometry and thermal states*, J. Phys. A: Math. Theor. **50**, 164001(18) (2017), doi:[10.1088/1751-8121/aa6268](https://doi.org/10.1088/1751-8121/aa6268).

[8] E. Tonni, J. Rodríguez-Laguna and G. Sierra, *Entanglement Hamiltonian and entanglement contour in inhomogeneous 1D critical systems*, J. Stat. Mech.-Theory E. **2018**, 043105(39) (2018), doi:[10.1088/1742-5468/aab67d](https://doi.org/10.1088/1742-5468/aab67d).

[9] E. Lieb, T. Schultz and D. Mattis, *Two soluble models of an antiferromagnetic chain*, Ann. Phys. **16**, 407 (1961), doi:[10.1016/0003-4916\(61\)90115-4](https://doi.org/10.1016/0003-4916(61)90115-4).

[10] F. Finkel and A. González-López, *Inhomogeneous XX spin chains and quasi-exactly solvable models*, J. Stat. Mech.-Theory E. **2020**, 093105(41) (2020), doi:[10.1088/1742-5468/abb237](https://doi.org/10.1088/1742-5468/abb237).

[11] P. Jordan and E. Wigner, *Über das Paulische Äquivalenzverbot*, Z. Physik **47**, 631 (1928), doi:[10.1007/BF01331938](https://doi.org/10.1007/BF01331938).

[12] G. Vidal, J. I. Latorre, E. Rico and A. Kitaev, *Entanglement in quantum critical phenomena*, Phys. Rev. Lett. **90**, 227902(4) (2003), doi:[10.1103/PhysRevLett.90.227902](https://doi.org/10.1103/PhysRevLett.90.227902).

[13] I. Peschel, *Calculation of reduced density matrices from correlation functions*, J. Phys. A: Math. Gen **36**, L205 (2003), doi:[10.1088/0305-4470/36/14/101](https://doi.org/10.1088/0305-4470/36/14/101).

[14] J. I. Latorre and A. Riera, *A short review on entanglement in quantum spin systems*, J. Phys. A: Math. Theor. **42**, 504002(33) (2009), doi:[10.1088/1751-8113/42/50/504002](https://doi.org/10.1088/1751-8113/42/50/504002).

[15] A. Rényi, *Probability Theory*, North-Holland, Amsterdam (1970).

[16] F. Finkel and A. González-López, *Entanglement entropy of inhomogeneous XX spin chains with algebraic interactions*, J. High. Energy Phys. **12**, 184(34) (2021), doi:[10.1007/JHEP12\(2021\)184](https://doi.org/10.1007/JHEP12(2021)184).

[17] B. Mula, N. Samos Sáenz de Buruaga, G. Sierra, S. N. Santalla and J. Rodríguez-Laguna, *Depletion in fermionic chains with inhomogeneous hoppings*, Phys. Rev. B **106**, 224204(10) (2022), doi:[10.1103/PhysRevB.106.224204](https://doi.org/10.1103/PhysRevB.106.224204).

[18] G. Ramírez, J. Rodríguez-Laguna and G. Sierra, *Entanglement over the rainbow*, J. Stat. Mech.-Theory E. **2015**, 06002(20) (2015), doi:[10.1088/1742-5468/2015/06/P06002](https://doi.org/10.1088/1742-5468/2015/06/P06002).

[19] N. Crampé, R. I. Nepomechie and L. Vinet, *Free-fermion entanglement and orthogonal polynomials*, J. Stat. Mech.-Theory E. **2019**, 093101(17) (2019), doi:[10.1088/1742-5468/ab3787](https://doi.org/10.1088/1742-5468/ab3787).

[20] G. Blanchet, G. Perez and L. Vinet, *Fermionic logarithmic negativity in the Krawtchouk chain*, J. Stat. Mech.-Theory E. **2024**, 113101(24) (2024), doi:[10.1088/1742-5468/ad84d8](https://doi.org/10.1088/1742-5468/ad84d8).

[21] P-A. Bernard, N. Crampé, Q. Labriet, L. Morey and L. Vinet, *Exactly solvable inhomogeneous XY spin chain*, J. Stat. Mech.-Theory E. **2025**, 103101(12) (2025), doi:[10.1088/1742-5468/ae0429](https://doi.org/10.1088/1742-5468/ae0429).

[22] R. B. Dingle and G. J. Morgan, *WKB methods for difference equations I*, Appl. Sci. Res. **18**, 221 (1967), doi:[10.1007/BF00382348](https://doi.org/10.1007/BF00382348).

[23] F. W. J. Olver, D. W. Lozier, R. F. Boisvert and C. W. Clark, eds., *NIST Handbook of Mathematical Functions*, Cambridge University Press (2010).

[24] S. Gershgorin, *Über die Abgrenzung der Eigenwerte einer Matrix*, Izv. Akad. Nauk SSSR Ser. Mat. **6**, 749 (1931).

[25] V. Eisler and I. Peschel, *Properties of the entanglement Hamiltonian for finite free-fermion chains*, J. Stat. Mech.-Theory E. **2018**, 104001(17) (2018), doi:[10.1088/1742-5468/aace2b](https://doi.org/10.1088/1742-5468/aace2b).

[26] J. Friedel, *Metallic alloys*, Nuovo Cimento Suppl. (1955–1965) **7**, 287 (1958), doi:doi.org/10.1007/BF02751483.

[27] R. Koekoek, P. Lesky and R. Swarttouw, *Hypergeometric Orthogonal Polynomials and their q -Analogues*, Springer-Verlag, Berlin, doi:[10.1007/978-3-642-05014-5](https://doi.org/10.1007/978-3-642-05014-5) (2010).

[28] G. Ramírez, J. Rodríguez-Laguna and G. Sierra, *From conformal to volume law for the entanglement entropy in exponentially deformed critical spin 1/2 chains*, J. Stat. Mech.-Theory E. **2014**, P10004(15) (2014), doi:[10.1088/1742-5468/2014/10/P10004](https://doi.org/10.1088/1742-5468/2014/10/P10004).

[29] I. MacCormack, A. Liu, M. Nozaki and S. Ryu, *Holographic duals of inhomogeneous systems: the rainbow chain and the sine-square deformation model*, J. Phys. A: Mat. Theor. **52**, 505401(24) (2019), doi:[10.1088/1751-8121/ab3944](https://doi.org/10.1088/1751-8121/ab3944).

[30] A. Szabó, *Rainbow chains and numerical renormalisation group for accurate chiral conformal spectra*, SciPost Phys. **19**, 075(30) (2025), doi:[10.21468/scipostphys.19.3.075](https://doi.org/10.21468/scipostphys.19.3.075).

[31] C. Holzhey, F. Larsen and F. Wilczek, *Geometric and renormalized entropy in conformal field theory*, Nucl. Phys. B **424**, 443 (1994), doi:[10.1016/0550-3213\(94\)90402-2](https://doi.org/10.1016/0550-3213(94)90402-2).

[32] P. Calabrese and J. Cardy, *Entanglement entropy and quantum field theory*, J. Stat. Mech.-Theory E. **2004**, P06002(27) (2004), doi:[10.1088/1742-5468/2004/06/P06002](https://doi.org/10.1088/1742-5468/2004/06/P06002).

[33] M. Fagotti and P. Calabrese, *Universal parity effects in the entanglement entropy of XX chains with open boundary conditions*, J. Stat. Mech.-Theory E. **2011**, P01017(26) (2011), doi:[10.1088/1742-5468/2011/01/P01017](https://doi.org/10.1088/1742-5468/2011/01/P01017).